Ionics
https://doi.org/10.1007/s11581-025-06566-w

RESEARCH

Parameter extraction of proton exchange membrane fuel cell using differential evolution–based artificial rabbits optimization

Manish Kumar Singla[1,2] · Mohammad Aljaidi[3] · Pradeep Jangir[4,5] · Arpita[1] · Ramesh Kumar[6] · Reena Jangid[7,8]

Received: 19 April 2025 / Revised: 7 July 2025 / Accepted: 15 July 2025

Abstract

Proton exchange membrane fuel cells (PEMFCs) are an important technology of clean energy because of their efficiency, low emissions and the ability to start up quickly. To achieve accurate performance predictions, it is crucial to have precise parameter estimation to come up with accurate PEMFC models. This paper proposes a new hybrid optimization algorithm, differential evolution-based artificial rabbits optimization (DEARO), with the specific purpose of extracting the seven main unknown parameters in PEMFC models. The DEARO algorithm suggested is a strategic combination of the advantages of differential evolution (DE) and artificial rabbits optimization (ARO) to address the shortcomings of the current approaches. The DEARO algorithm proposes three major novelties an adaptive mutation mechanism which combines several DE strategies (DE/rand/1, DE/best/1 and DE/rand/2) to provide global search capabilities and prevent premature convergence, a dynamic crossover operation which intelligently combines the characteristics of the solutions to improve local refinement and a failure rate–based adaptation scheme that automatically adapts the control parameters to maintain the best balance between exploration and exploitation during the optimization process. The features allow DEARO to effectively traverse the multimodal, multimodal search space that is typical of PEMFC parameter estimation problems. The validation was carried out comprehensively with 12 different PEMFC stacks of the major manufacturers, such as BCS 500W, NedStack PS6, and Ballard Mark V systems. The experimental findings prove that DEARO is more accurate with SSE being up to 92.5% lower than traditional approaches (e.g. 0.0255 vs 0.0412 in the case of BCS 500W). The statistical analysis of 40 independent runs showed an outstanding consistency with standard deviations as low as $5.9110-5$. The computational efficiency of the algorithm is also impressive with most test cases being solved to optimal solutions within 0.4 s and with a robust performance in a wide range of operating conditions. The results of comparative studies with nine state-of-the-art algorithms (RUN, HHO, RIME and PSO) proved the advantage of DEARO in terms of accuracy and reliability. Convergence analysis demonstrated that DEARO usually converges to optimal solutions in less than 50 iterations, which is a lot faster compared to other methods. Further confirmation of the effectiveness of the algorithm is made by I-V/P–V characteristic matching, boxplot analyses and non-parametric statistical tests. The developments make DEARO an effective means of designing, optimizing and real-time controlling PEMFC systems and possibly other complex energy system modelling problems.

Keywords Proton exchange membrane fuel cell · Optimization · Differential evolution · Artificial rabbit's optimization · Hydrogen cell

Introduction

Proton exchange membrane fuel cells (PEMFCs) are promising energy sources, generating clean, renewable power [1]. Characterized by high energy efficiency and environmentally friendly operation, they hold considerable potential for various real-world applications. Despite the considerable potential of PEMFCs in various applications, realizing their peak performance is strongly tied to their design and operational parameters. The design of a PEMFC encompasses a multitude of parameters, such as flow field type, catalyst volume, rib and channel design, clamping force, width and component hydrophobicity/quality [2]. These parameters typically have both minor and major effects during cell fabrication [3]. Nevertheless, after the construction of a stack or single cell, and setting aside the initial engineering aspects, identifying the optimal operational parameters has become a crucial modern strategy for performance improvement. As

Extended author information available on the last page of the article

Published online: 13 August 2025

a result, numerous numerical and experimental studies have investigated the impact of operating constraints on PEMFC output [4].

Fuel cells (FCs), beyond their application in PEMFCs, are generally recognized as highly efficient electrochemical devices for direct power generation from fuel. Their electrochemical conversion process offers a productive environment and favourable energy transformation, establishing them as a universally recognized modern power source [5]. As a result, they have attracted considerable interest and experienced rapid growth in industrial stationary power, domestic applications and transportation, with their low operating temperature and a set of unique advantages: high power density, safe and precise operation and compact design. PEMFCs are a standout among various fuel cell types [6]. Studies reveal that PEMFCs perform best with a flow rate between 1000 and 1600 ml/min, at an ideal operating temperature of roughly 69.9 °C and within an efficient temperature range of 60 to 80 °C [7].

Capitalizing on these benefits, PEMFCs are being extensively evaluated for use in vehicles and power equipment requiring low-temperature operation and high energy density. Current PEMFC research centres on modelling and investigating the interplay of various subsystems to enhance energy quality and overall system output [8]. A notable example is the integration of photovoltaics with proton exchange membrane hydrogen production, which presents a compelling solar energy storage solution by transforming excess photovoltaic energy into a long-term, low-power transmission source with minimal frequency demands and zero pollution [9]. While the PEMFC technology has advanced, designing the polarization trajectory for specific PEMFCs poses considerable challenges, especially in precisely specifying the numerous adjustment parameters [10]. Moreover, the frequent use of real PEMFC production makes it difficult to accurately determine the parameters within the designed model [6]. This makes parameter estimation an optimization engineering problem where current optimizers can struggle to find precise adjustment parameter values due to insufficient information, resulting in significant errors [11]. Over the past few years, various optimization algorithms have been employed in the literature to estimate the parameters of PEMFC models [12].

A significant problem is the frequent omission of numerous adjustment parameters in PEMFC datasheets. Therefore, identifying these parameters is essential for building a precise and complete model [13]. This paper focuses on extracting the optimal values of these datasheet-missing PEMFC model parameters, specifically those required to generate polarization curves that closely align with test data. Obtaining these parameters will facilitate the rapid development of satisfactory mathematical PEMFC models for researchers. The optimization strategy involves minimizing a fitness function that quantifies the squared difference between simulated and experimental stack voltage. To achieve this, this article introduces an enhanced method that integrates two recent optimization algorithms for the effective determination of PEMFC model parameters.

While PEMFC technology has seen significant advancements recently, its associated costs have created disagreements between its supporters and detractors [14]. Nonetheless, improving the effectiveness of PEMFCs is critical for their commercial prospects and achieving significant market penetration. Since end-user recognition is a fundamental aspect of FCs, examining how operational parameters influence their performance is essential. The effectiveness of a PEMFC is ultimately governed by various operational and adjustment parameters, and numerous studies have focused on its development using different optimization methods. Seleem et al. [15] proposed a new, accurate and simplified PEMFC model with four parameters, utilizing the integral squared error as the objective function and innovatively employing the equilibrium optimizer to determine the unknown parameters. Their method demonstrated high effectiveness under both dynamic and steady-state conditions, resulting in accurate model parameters. The authors of [16] presented a comparative study to analyse the impacts of adjusting PEMFC parameters, in addition to providing a structural overview and modelling approach. Furthermore, their investigation aimed to explore various control and clarification techniques for FC components to identify the best ways to enhance performance. Following various optimization approaches, stochastic methods have become significant tools for exploring the solution landscape and seeking near-optimal results [17]. Meta-heuristic techniques are the most prevalent within stochastic methods, offering benefits like straightforward implementation, simplicity, flexibility and freedom from specific problem limitations [18]. In recent years, many meta-heuristic algorithms have been proposed to address intricate optimization challenges, capable of finding near-optimal solutions with sufficient accuracy in a practical amount of time. Meta-heuristics have been successfully applied across numerous research domains, including Bioinformatics [19, 20], Engineering Control [21–23], solar cell parameter extraction [24, 25], Mechanical suspension systems [26], Cross-Docking systems [27] and Digital Watermarking [28].

Mathematical models that represent PEMFC behaviour incorporate equations detailing the electrochemical processes within the cell and their dependence on unknown parameters. Meta-heuristic algorithms are used to search the parameter space and pinpoint the combination of values that minimizes a predetermined objective function, often the sum of squared errors. The goal is to develop an optimization strategy that converges effectively to optimal parameter values while addressing the inherent computational complexities. By refining the accuracy of these parameter estimations, this

research aims to enhance the performance and efficiency of PEMFCs in real-world applications. For PEMFC optimization, Ali et al. [29] proposed a novel application of the grey wolf optimizer (GWO) in their PEMFC-GWO model. This approach yielded highly competitive results when compared to other well-known methods in the literature. Moreover, the Slime Mould Algorithm (SMA) was utilized to optimize the selection of parameters for PEMFCs [30]. In a separate study [31], the Coyote Optimization Algorithm (COA) was applied to tune the parameters of two distinct FC modules: the 50 W stack and the Ned Stack PS6, using the sum squared error as the fitness metric. Furthermore, the depth information-based differential evolution algorithm was employed to estimate the parameters of 12 different PEMFCs [32]. Finally, the artificial hummingbird algorithm, improved with Lévy flight, was investigated for its ability to determine the parameters of seven PEMFC case studies [33].

To estimate PEMFC parameters, a hybrid meta-heuristic algorithm integrating Harris Hawk Optimization (HHO) and Atom Search Optimization (ASO) was developed [34]. This algorithm was experimentally validated on three commercial modules: 500 W SR-12, BCS 500 W and a 250 W stack. Similarly, a modified fluid search optimization algorithm was created for the precise estimation of PEMFC parameters, with experimental tests conducted on the BCS 500 W and NedStack PS6 modules [35]. The Flower Grey INFO Naked (FGIN) algorithm, employing multiple strategies and algorithms, was utilized to determine the optimal values of seven unknown parameters for five different PEMFC stacks [36]. Furthermore, a hybrid approach combining the vortex search algorithm (VSA) and DE algorithms was presented in [37] for fuel cell parameter estimation, applied to four modules: NedStack PS6, a 250 W stack, BCS 500-W and SR-12 PEM 500 W. An enhanced Arithmetic Optimization algorithm, incorporating opposition-based learning, was also developed for PEMFC parameter estimation [38]. Lastly, the Kepler Red Meerkat Grey (KRMG) algorithm, another multi-hybrid approach, was evaluated for identifying parameters in three distinct PEMFC modules [39].

To estimate PEMFC parameters, a new hybrid method called INFONM, based on weighted mean of vectors and Nelder-Mead, was assessed on four benchmark PEMFCs, estimating seven parameters each [40]. The educational competition optimizer (ECO) was also utilized to estimate the steady-state model parameters for three PEMFCs [41]. An ensemble approach combining sinusoidal parameter adaptation and L-SHADE integration was applied in another study [42] to estimate PEMFC parameters for the SR-12, 500 W; NedStack PS6, 6 kW; 250 W and BCS 500 W modules. In addition to these, numerous other optimization techniques have been investigated for the optimal estimation of PEMFC parameters, including a combination of artificial bee colony with differential evolution shuffled complex [43], shuffled multi-simplexes search algorithm [44], Enhanced Slime Mold Algorithm [45], heap-based optimization algorithm [46], Barnacles Mating Optimization algorithm [47], enhanced Archimedes optimization algorithm [48], gradient-based optimizer [49], Artificial Rabbits Optimization Algorithm [50], enhanced fluid search optimization algorithm [35], moth-flame optimization [51], Dandelion Optimizer [52], Jellyfish search algorithm [53], chaotic binary shark smell optimizer [54], an improved gorilla troops technique [55] and a hybrid sine–cosine crow search algorithm [14].

Instead of just combining meta-heuristic algorithms, research has also focused on improving the performance of individual algorithms, akin to ensemble methods in machine learning. Such enhancements can guide the search process by offering a wider range of solutions or directing it to potentially optimal regions [56, 57]. This diversity is crucial for balancing exploration (searching a broad solution space) and exploitation (intensifying the search in promising areas) within metaheuristic optimization. Additionally, the augmented Lagrangian approach, which addresses constrained optimization by integrating Lagrangian relaxation with penalty functions through iterative updates of Lagrange multipliers and optimization of an augmented objective function, can effectively work in tandem with meta-heuristics for problem-solving [58, 59]. However, the No-Free-Lunch (NFL) theorem posits that no single meta-heuristic algorithm excels at solving all engineering optimization problems with the highest efficiency.

By integrating essential differential evolution (DE) mechanisms into the artificial rabbits algorithm (ARO), DEARO aims to achieve superior optimization performance, particularly in demanding tasks like PEMFC parameter estimation. This is accomplished through three DE-inspired mutation strategies that enhance population diversity and help escape local optima, the implementation of binomial crossover for effectively combining beneficial solution characteristics to improve exploitation and an adaptive control of the crossover rate and scale factor, guided by a failure rate metric, to dynamically balance exploration and exploitation throughout the search, ultimately leading to more accurate and robust parameter identification than the original ARO [60]. The DEARO test was used to find the optimal settings for 12 different PEM fuel cell systems, which are known to be very complex and nonlinear. The results showed that DEARO was really fast and accurate at finding those optimal settings. This makes it a powerful tool for improving PEM fuel cell technology and helping us use them more effectively in energy and transportation.

The proposed DEARO algorithm represents a significant advancement in PEMFC parameter optimization through three primary contributions. First, the integration of differential evolution (DE) mechanisms into the ARO framework enhances both exploration and exploitation capabilities. Specifically, DEARO incorporates three distinct DE-inspired mutation

strategies to improve population diversity and escape local optima, a critical limitation of conventional ARO. Second, the implementation of binomial crossover enables more effective recombination of solution characteristics, facilitating accelerated convergence toward optimal parameter values. This hybridization addresses the inherent trade-off between global search breadth and local refinement observed in standalone metaheuristics. Third, DEARO introduces an adaptive control mechanism for crossover rates and scale factors, dynamically guided by a failure rate metric. This self-tuning capability allows the algorithm to autonomously balance exploration and exploitation throughout the optimization process, a feature absent in both classical DE and ARO variants. These algorithmic innovations collectively enable DEARO to achieve superior accuracy in identifying the seven critical PEMFC parameters (ξ_1, ξ_2, ξ_3, ξ_4, λ, R_C, b) compared to existing approaches. The validation across 12 commercial PEMFC stacks demonstrates consistent improvements in both solution quality (evidenced by reduced SSE values) and computational efficiency (faster convergence rates), establishing DEARO as a robust tool for fuel cell modelling and simulation.

The contributions of this research are summarized as follows:

- Application to PEMFCs: The DEARO algorithm is applied to optimize design variables for six PEMFC stacks: BCS 500 W [61, 62], SR-12 500 W [61, 62], STD 250 W [61] [62], Nedstack 600 W PS6 [62], Horizon H-12 [63] and Ballard Mark V [64].
- Comparative analysis: The performance of DEARO is benchmarked against nine state-of-the-art algorithms, including RUN algorithm (RUN) [65], Harris Hawks optimization (HHO) [66], RIME algorithm (RIME) [67], JAYA algorithm (JAYA) [68], TEO optimization (TEO) [69], INFO optimization (INFO) [70], moth flame optimizer (MFO) [71], Aquila Optimizer (AO) [72] and particle swarm optimization (PSO) [73], across a range of optimization scenarios.
- Environmental impact assessment: The impact of varying temperature and pressure conditions on PEMFC performance is evaluated, demonstrating the adaptability and reliability of the optimized models.
- Validation against experimental data: Simulation results are validated against experimental data for each PEMFC stack, confirming the robustness and accuracy of the DEARO optimized models.

This paper is structured as follows: "Mathematical modelling of PEMFC" details the PEMFC mathematical model, including design variables and optimization objectives. "Algorithm" introduces the differential evolution–based artificial rabbits optimization (DEARO), explaining its features and implementation. "Results analysis and discussion" presents simulation results and a comparison with other algorithms. "Conclusion" concludes the paper, summarizing contributions and outlining future research directions.

Mathematical modelling of PEMFC

Basic concept

The essential architecture of a PEMFC is characterized by an anode and a cathode, separated by a proton-conducting membrane acting as the solid polymer electrolyte. A schematic of this configuration is presented in Fig. 1.

The membrane's selective permeability, allowing proton conduction while impeding electron transfer [74], is fundamental. Catalyst layers are employed to enhance the kinetics of the electrochemical reactions. Hydrogen gas, supplied to the anode, undergoes catalytic dissociation, yielding protons and electrons. Protons are transported across the membrane to the cathode catalyst layer, while electrons are directed through an external electrical circuit. In parallel, an oxygen-containing gas (oxygen or air) is introduced to the cathode. At the cathode catalyst layer, oxygen undergoes electrochemical reduction by reacting with protons transported across the membrane and electrons supplied via the external circuit, yielding water. The electrochemical reactions occurring at the PEMFC electrodes are represented by the following Eqs. 1 to 3 [74]:

Anode reaction

$$H_2 \rightarrow 2H^+ + 2e^- \tag{1}$$

Cathode reaction

$$2H^+ + \tfrac{1}{2}O_2 \rightarrow H_2O \tag{2}$$

Overall reaction:

$$H_2 + \tfrac{1}{2}O_2 \rightarrow H_2O + \text{Energy} + \text{Heat} \tag{3}$$

The 'Energy' term in Eq. (3) corresponds to the electrical work performed by the electrons, derived from the electrochemical oxidation of hydrogen gas at the anode, as they traverse an external load to reach the cathode.

PEMFC stacks mathematical model

To determine the voltage generated by each individual fuel cell V_{cell}, the following expression is employed in Eq. 4 [75, 76]:

$$V_{cell} = E_{nerst} - \Delta V_{act} - \Delta V_{ohm} - \Delta V_{con} \tag{4}$$

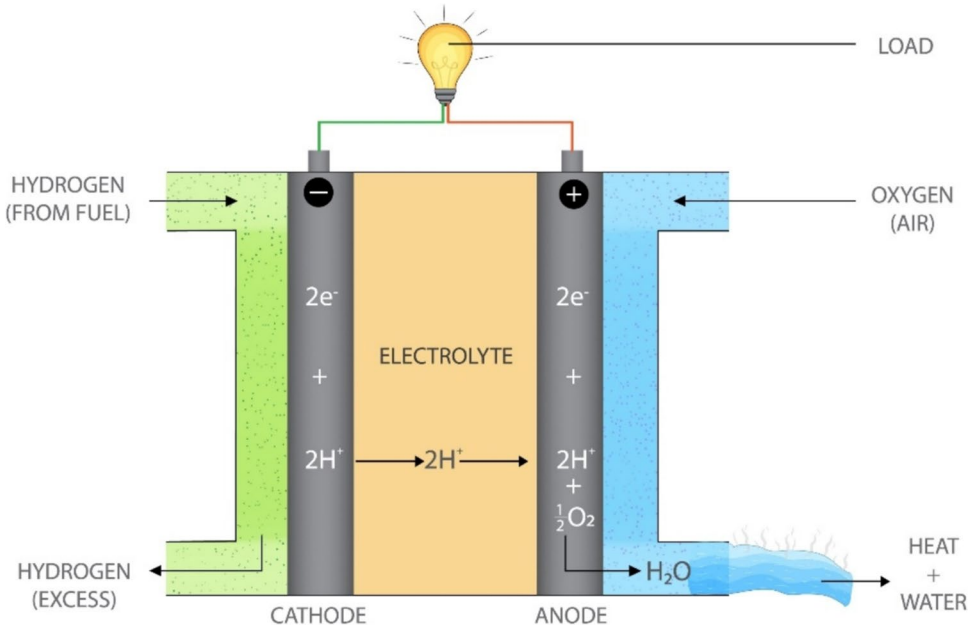

Fig. 1 Schematic diagram of PEMFC

The equation is composed of: E_{nerst}, representing the thermodynamic open-circuit potential; ΔV_{act}, the activation polarization loss; ΔV_{ohm}, the resistive polarization loss due to electronic and ionic conduction; and ΔV_{con}, the concentration polarization loss. Utilizing the electrochemical model proposed by Amphlett et al. [77], the total stack voltage, resulting from a series arrangement of N_{cells} identical fuel cells, is determined by Eq. 5:

$$V_{\text{stack}} = N_{\text{cells}} \cdot V_{\text{cell}} \tag{5}$$

In this equation, N_{cells} represents the number of fuel cells in the series, and V_{cell} is the voltage of a single cell, as defined by Eq. 4.

The determination of the reversible potential, denoted as E_{nerst}, is achieved through the subsequent expressed in Eq. 6 [8, 78]:

$$E_{\text{nerst}} = 1.229 - 8.5 \times 10^{-4}(T_{\text{fc}} - 298.15) + 4.3085 \times 10^{-5} T_{\text{fc}} \cdot \left[\ln(P_{\text{H}_2}) + \ln\left(\sqrt{P_{\text{O}_2}}\right)\right] \tag{6}$$

The cell's absolute operating temperature (T_{fc}, in Kelvin) and the partial pressures of hydrogen P_{H_2} and oxygen P_{O_2}, in atmospheres are used in this equation. For a hydrogen-air fuel cell, the oxygen partial pressure P_{O_2} is determined by the following Eq. 7 [79, 80]:

$$P_{\text{O}_2} = P_{\text{c}} - RH_{\text{c}} P^{\text{sat}}_{\text{H}_2\text{O}} - \frac{0.79}{0.21} P_{\text{O}_2} \cdot exp\left(0.291 \frac{I_{\text{fc}}}{A} / T^{0.832}_{\text{fc}}\right) \tag{7}$$

The following variables are employed: P_{c}, the cathode inlet manifold pressure (atm); RH_{c}, the cathode electrode relative humidity; I_{fc}, the operating current (amperes); A, the membrane active area (cm^2); and $P^{\text{sat}}_{\text{H}_2\text{O}}$, the saturation water vapor pressure, which is defined by the subsequent relationship given in Eq. 8 [81]:

$$\log_{10}(P^{\text{sat}}_{H_2O}) = 2.95 \times 10^{-2}(T_{\text{fc}} - 273.15) - 9.18 \times 10^{-5}(T_{\text{fc}} - 273.15)^2 + 1.44 \times 10^{-7}(T_{\text{fc}} - 273.15)^3 - 2.18 \tag{8}$$

In scenarios employing hydrogen and pure oxygen as reactants, the partial pressure of oxygen, denoted as P_{O_2}, is determined according to the subsequent expression given in Eq. 9 [82]:

$$P_{\text{O}_2} = RH_{\text{c}} P^{\text{sat}}_{\text{H}_2\text{O}} \left[\left(\exp\left(4.192 \frac{1}{I_{\text{fc}}} / T^{1.334}_{\text{fc}}\right) \cdot \frac{RH_{\text{c}} P^{\text{sat}}_{\text{H}_2\text{O}}}{P_{\text{a}}}\right)^{-1} - 1\right] \tag{9}$$

In all instances, the partial pressure of hydrogen, denoted as P_{H_2}, is expressed by Eq. 10:

$$P_{H_2} = 0.5 RH_{\text{a}} P^{\text{sat}}_{H_2O} \left[\left(\exp\left(1.635 \frac{1}{I_{\text{fc}}} / T^{1.334}_{\text{fc}}\right) \cdot \frac{RH_{\text{a}} P^{\text{sat}}_{H_2O}}{P_{\text{a}}}\right)^{-1} - 1\right] \tag{10}$$

P_{a} denotes the anode electrode inlet channel pressure, expressed in atmospheres, and RH_{a} signifies the relative humidity pertaining to the anode side.

The following formula calculates the activation voltage drop, ΔV_{act} is given in Eq. 11:

$$\Delta V_{act} = -\left[\xi_1 + \xi_2 T_{fc} + \xi_3 T_{fc} \ln(C_{O_2}) + \xi_4 T_{fc} \ln(I_{fc})\right] \quad (11)$$

The terms ξ_1, ξ_2, ξ_3, and ξ_4 are empirical parameters, and C_{O_2} denotes the oxygen concentration at the cathode catalyst layer, expressed in mol/cm^3, defined in Eq. 12:

$$C_{O_2} = \frac{P_{O_2}}{5.08\times10^6 \cdot \exp(-498/T_{fc})} \quad (12)$$

The following Eq. 13 determines the ohmic resistive voltage drop, ΔV_{ohm}:

$$\Delta V_{ohm} = I_{fc}(R_M + R_C) \quad (13)$$

The terms R_M and R_C denote the membrane resistance (ohms) and the protonic resistance across the membrane, respectively. The membrane resistance, R_M, is determined in Eq. 14:

$$R_M = \frac{\rho_M \cdot l}{A} \quad (14)$$

The variables ρ_M and l denote the specific membrane resistivity (Ω·cm) and membrane thickness (cm), respectively. The empirical relationship for determining ρ_M is determined in Eq. 15:

$$\rho_M = \frac{181.6\left[1 + 0.03\left(\frac{I_{fc}}{A}\right) + 0.062\left(\frac{T_{fc}}{303}\right)^2\left(\frac{I_{fc}}{A}\right)^{2.5}\right]}{\left[\lambda - 0.634 - 3\left(\frac{I_{fc}}{A}\right)\right] \times \exp\left[4.18\left(\frac{T_{fc}-303}{T_{fc}}\right)\right]} \quad (15)$$

where λ is an adjustable parameter that depends on the membrane fabrication process.

The concentration voltage drop, ΔV_{con}, is determined by the following formula in Eq. 16:

$$\Delta V_{con} = -b\ln\left(1 - \frac{J}{J_{max}}\right) \quad (16)$$

The term 'b' denotes a parametric coefficient, expressed in volts, while J and J_{max} represent the operating and limiting current densities, respectively, both in units of amperes per square centimetre.

To achieve fidelity in simulation and control modelling, precise parameter identification is imperative. The proposed optimization methodology is utilized to determine the optimal values of the seven unknown parameters: $\xi_1, \xi_2, \xi_3, \xi_4, \lambda, R_C$ and b.

Objective function

To ensure the model's results closely match real-world PEMFC experiments, researchers used an optimization method. This method works by reducing the difference between the model's voltage predictions and the voltages measured in experiments [29]. Specifically, they minimized the sum of squared errors (SSEs) between these two sets of voltage values is given in Eq. 17:

$$\mathrm{OF} = min\mathrm{SSE}(x) = min\sum_{i=1}^{N}[v_{meas}(i) - v_{cal}(i)]^2 \quad (17)$$

The term x represents the vector of unknown model parameters, N is the cardinality of the dataset, i is the iteration index, v_{meas} is the experimentally determined PEMFC voltage, and v_{cal} is the model-predicted voltage. The optimization problem is subject to the following constraints is given in Eq. 18:

$$\begin{aligned} &\xi_{i,\min} \le \xi_i \le \xi_{i,\max}, i = 1:4 \\ &R_{C\min} \le R_C \le R_{C\max} \\ &\lambda_{\min} \le \lambda \le \lambda_{\max} \\ &b_{\min} \le b \le b_{\max} \end{aligned} \quad (18)$$

The constraints are defined by $\xi_{i,\min}$ and $\xi_{i,\max}$, the lower and upper bounds of the empirical coefficients; $R_{C,\min}$ and $R_{C,\max}$, the minimum and maximum values for the resistance, and $\lambda_{\min}$, $\lambda_{\max}$, $b_{\min}$ and $b_{\max}$, the respective lower and upper bounds for the water content and parametric coefficients. The mean bias error of the voltage is quantified using the subsequent expression in Eq. 19:

$$MBE = \frac{\sum_{i=1}^{N}|V_{meas}(i) - V_{calc}(i)|}{N} \quad (19)$$

Algorithm

Classical DE algorithm

Recognizing the significant advancements in differential evolution (DE) research and its broad applications in various scientific and technological areas, this section presents an overview of the classical DE algorithm [83, 84]. The fundamental principle behind DE is to use the variations between individuals in a population to guide the search within the solution space. This process primarily involves four key stages: initialization, mutation, crossover and selection. A clear understanding of these steps is essential to appreciate the subsequent improvements and modifications developed for DE.

The differential evolution (DE) algorithm commences with a randomly generated initial population. A novel solution is produced by taking a third population member and adding to it a scaled vector representing the difference between two other randomly selected members. This newly formed solution then enters a competition with its original counterpart,

and the individual with the better fitness is chosen for the subsequent iteration. Across numerous generations, this mechanism of retaining high-performing individuals and discarding lower-performing ones progressively steers the search process toward the optimal solution. The fundamental evolutionary operations in DE are described below.

Initialization

The DE algorithm initializes a solution using a D-dimensional vector (M). For a given population size (N), each individual can be expressed as: $x_{i,G} = (x_{i1}\,(G), x_{i2}\,(G), \ldots, x_{iD}\,(G))$. The initial population is generated within the range $[x_{\min}, x_{\max}]$. The relationship is represented in Eq. 20:

$$x_{iD} = x_{\min} + \text{rand}(0,1) \cdot (x_{\max} - x_{\min}) \tag{20}$$

Here, G represents the generation, $x_{\max}$ and $x_{\min}$ denote the maximum and minimum values of the search space, respectively, and rand(0,1) refers to a random number uniformly distributed within the interval (0, 1).

Mutation

The mutation process in the DE algorithm generates a mutation vector, $V_{i,G}$, for each individual, $x_{i,G}$, in the current population (target vector). The mutation strategy is typically expressed as DE/x/y, where x indicates the base vector, and y specifies the number of difference vectors utilized. The five widely recognized mutation strategies are described in following Eqs. 17 to 25:

1. DE/rand/1

$$V_{i,G} = x_{r_1,G} + F \cdot (x_{r_2,G} - x_{r_3,G}) \tag{21}$$

2. DE/best/1

$$V_{i,G} = x_{\text{best},G} + F \cdot (x_{r_1,G} - x_{r_2,G}) \tag{22}$$

3. DE/rand-to-best/1

$$V_{i,G} = x_{i,G} + F \cdot (x_{\text{best},G} - x_{i,G}) + F \cdot (x_{r_1,G} - x_{r_2,G}) \tag{23}$$

4. DE/best/2

$$V_{i,G} = x_{\text{best},G} + F \cdot (x_{r_1,G} - x_{r_2,G}) + F \cdot (x_{r_3,G} - x_{r_4,G}) \tag{24}$$

5. DE/rand/2

$$V_{i,G} = x_{i,G} + F \cdot (x_{r_1,G} - x_{i,G}) + F \cdot (x_{r_2,G} - x_{r_3,G}) \tag{25}$$

In the above equations, r_1, r_2, r_3, r_4 and r_5 are unique integers randomly selected within $[1, M]$. The scale factor F serves as a control parameter to amplify the difference vector, while $x_{\text{best},G}$ represents the best individual vector in the population at generation G.

Crossover

The binomial crossover operator in the DE algorithm facilitates the generation of trial vectors, $u_{i,G}$, by combining the mutation vector, $v_{i,G}$, and the target vector, $x_{i,G}$. Trial vectors are produced based on the following relationship 26:

$$u_{i,G} = \begin{cases} v_{i,G}, & \text{if rand}_j(0,1) \le CR \text{ or } j = j_{\text{rand}}, j = 1,2,\ldots,D \\ x_{i,G}, & \text{otherwise} \end{cases} \tag{26}$$

Here, $\text{rand}_j(0,1)$ is a random number uniformly distributed within the interval (0,1), and CR refers to the crossover rate that determines the proportion of information inherited by the trial vector u_i from either the mutation vector v_i or the target vector x_i.

Selection

The selection process in DE involves assessing the fitness values of all newly generated trial vectors. For minimization tasks, each trial solution is directly compared against the current best solution within the population (the target vector). If the trial solution demonstrates equal or superior fitness, it supersedes the target vector. Conversely, if the target vector is fitter, it is retained for the next generation. This repeated comparison and replacement mechanism gradually improves the population over successive iterations. This selection logic can be mathematically represented in Eq. 27:

$$X_{i,G+1} = \begin{cases} U_{i,G}, & \text{if } f(U_{i,G}) \le f(X_{i,G}) \\ X_{i,G}, & \text{otherwise} \end{cases} \tag{27}$$

By prioritizing the survival of the fittest individuals, this greedy selection mechanism effectively facilitates the algorithm's convergence towards an optimal solution.

ARO

Drawing inspiration from the survival planning of rabbits in the natural world [85], ARO is a newly developed nature-inspired meta-heuristic optimization algorithm. The exploratory behaviour of the ARO algorithm is managed through the use of the following Eq. 28:

$$\vec{v}_i(t+1) = \vec{x}_j(t) + R \cdot \left(\vec{x}_i(t) - \vec{x}_j(t)\right) + \text{round}\left(0.\left(0.05 + r_1\right)\right) \cdot n_1 \tag{28}$$

where the indices i and j take integer values from 1 to n, and j is not equal to i. The vector $v_i\,(t+1)$ signifies the prospective location of the i^{th} rabbit at the subsequent time step, $t+1$. The vector $x_j\,(t)$ represents the current location of the

j^{th} rabbit at time t. The scalar r_1 is a random value within the interval (0,1), and n_1 is a random value drawn from a standard normal distribution. The variable n indicates the total number of rabbits in the population. The value of R is computed as following Eq. 29:

$$R = L \cdot c \tag{29}$$

In this equation, L is defined as $L = (e - e\ (1/\text{iter}_{\max})^2 \sin(2\pi r_2)$, with the condition that r_2 is a value within the range (0,1). Here, t refers to the present iteration count, and $\text{iter}_{\max}$ indicates the predefined maximum number of iterations. The coefficient c in Eq. 29 is calculated as Eq. 30:

$$c(k) = \begin{cases} 1, \ if\ k == g(1) \\ 0, otherwise \end{cases} k = 1, \ldots .d \text{ and } l = 1, \ldots .., \lceil r_3.d \rceil \tag{30}$$

Here, d indicates the dimension of the solution space being explored, r_3 is a random value within the interval (0,1), and g is a random index selected on the fly from a randomized ordering of the integers from 1 to d.

As a survival strategy against predators, rabbits dig numerous burrows near their nests for hiding. Similarly, in each iteration of the algorithm, each rabbit generates d potential hiding places (burrows) around its current location, one for each dimension of the search space, and then randomly selects one burrow to occupy. The location of the j^{th} burrow for the i^{th} rabbit is determined by Eq. 31:

$$\vec{b}_{i,j}(t) = \vec{x}_i(t) + H \cdot g \cdot \vec{x}_i(t) \tag{31}$$

where the rabbit index i ranges from 1 to n; the dimension index j ranges from 1 to d, and the parameter H, which depends on the current iteration t and the maximum iterations $\text{iter}_{\max}$, is calculated as $H = \text{iter}_{\max} - t + 1/\text{iter}_{\max}$ * r_4The value r_4 is a random number in the interval (0,1). The value of g in Eq. 31 is then determined as Eq. 32:

$$g(k) = \begin{cases} 1, \ if\ k == j \\ 0, otherwise \end{cases} k = 1, \ldots .., d \tag{32}$$

The random hiding mechanism of the rabbits is implemented through the following Eqs. 33 to 35:

$$\vec{v}_i(t+1) = \vec{x}_i(t) + R \cdot \left(r_4 \cdot \vec{b}_{i,r}(t) - \vec{x}_i(t) \right), i\epsilon(1,n) \tag{33}$$

$$\vec{b}_{i,r}(t) = \vec{x}_i(t) + H \cdot g_r \cdot \vec{x}_i(t) \tag{34}$$

$$g_r(k) = \begin{cases} 1, \ if\ k == \lfloor r_5 \cdot d \rfloor \\ 0, otherwise \end{cases} k =, \ldots \ldots, d \tag{35}$$

Here, $\vec{b}_{i,r}(t)$ signifies a burrow that the i^{th} rabbit randomly selects from its d burrows in the t^{th} iteration to hide. The value r_5 is a random number within the range (0,1). After

Table 1 Twelve PEMFC manufacturer sheets

S. No	SHEET 1	SHEET 2	SHEET 3	SHEET 4	SHEET 5	SHEET 6	SHEET 7	SHEET 8	SHEET 9	SHEET 10	SHEET 11	SHEET 12
PEMFC Type	BCS 500 W	NetStack PS6	SR-12	H-12–1	Ballard Mark V	STD −1	Horizon	STD −2	STD −3	STD −4	H-12–2	H-12–3
Power(W)	500	6000	500	12	5000	250	500	250	250	250	12	13
Ncells (no)	32	65	48	13	35	24	36	24	24	24	13	13
A(cm^2)	64	240	62.5	8.1	232	27	52	27	27	27	8.1	8.1
l(um)	178	178	25	25	178	127	25	127	127	127	25	25
T(K)	333	343	323	323	343	343	338	343	343	343	302	312
Jmax(mA/cm^2)	469	1125	672	246.9	1500	860	446	860	860	860	246.9	246.9
PH_2(bar)	1.0	1.0	1.47628	0.4935	1.0	1.0	0.55	1.5	2.5	2.5	0.4	0.5
PO_2(bar)	0.2095	1.0	0.2095	1.0	1.0	1.0	1.0	1.5	3.0	3.0	1.0	1.0

Table 2 Optimal parameter values and performance metrics

Algorithm	RUN	HHO	RIME	JAYA	TEO	INFO	MFO	AO	PSO	DEARO
ξ_1	−1.17583	−1.0582	−1.19969	−0.86523	−1.03313	−1.09728	−1.06638	−0.95861	−0.8867	−0.85343
ξ_2	0.003505	0.002796	0.004184	0.002236	0.003071	0.003796	0.003352	0.00318	0.002293	0.002206
ξ_3	5.86E−05	3.6E−05	0.000098	3.73E−05	5.86E−05	9.27E−05	7.02E−05	8E−05	3.69E−05	3.76E−05
ξ_4	−0.00019	−0.00019	−0.00019	−0.00019	−0.00019	−0.0002	−0.00019	−0.00019	−0.00019	−0.00019
λ	17.7761	22.14188	20.87725	22.41415	20.85853	22.36859	21.17813	20.93096	22.94963	20.87724
R_c	0.0001	0.000254	0.0001	0.000314	0.0001	0.0001	0.00013	0.0001	0.000465	0.0001
B	0.0136	0.01593	0.016126	0.015932	0.016115	0.017024	0.016152	0.016172	0.014101	0.016126
Min	0.041232	0.025791	0.025493	0.026208	0.025493	0.027982	0.025547	0.025499	0.042231	0.025493
Max	0.31018	0.039318	0.096279	0.035803	0.03698	0.045214	0.026145	0.027606	0.232804	0.025653
Mean	0.120996	0.031034	0.039666	0.030417	0.026788	0.033332	0.025683	0.025689	0.120083	0.025524
Std	0.081051	0.005165	0.016773	0.003357	0.002939	0.00547	0.000166	0.000532	0.060652	5.91E−05
RT	11.00805	18.91079	11.90938	12.48756	23.81196	13.7502	15.52803	14.13554	22.00453	0.386165
FR	9.466667	5.866667	6.8	6.066667	3.666667	6.6	3.533333	2.4	9.4	1.2

the rabbit performs both detour foraging and random hiding behaviours, its position is updated as following Eq. 36:

$$\vec{x}_i(t+1) = \begin{cases} \vec{x}_i(t), iff\left(\vec{x}_i(t)\right) \le f\left(\vec{v}_i(t+1)\right) \\ \vec{v}_i(t+1), iff\left(\vec{x}_i(t)\right) > f\left(\vec{v}_i(t+1)\right) \end{cases} \tag{36}$$

Here, $f\left(\vec{x}_i(t)\right)$ indicates the fitness of the $\vec{x}_i(t)$ candidate solution at iteration t. The algorithm's balance between exploring new regions of the search space and exploiting promising ones is managed by the control parameter $A(t)$, given by Eq. 37:

$$A(t) = 4\left(1 - \frac{t}{\text{iter}_{\max}}\right) ln\left(\frac{1}{r_6}\right) \tag{37}$$

Here, r_6 represents a random value within the interval (0,1). In the artificial rabbits optimization (ARO) algorithm, the condition $A(t) > 1$ triggers the exploration phase, whereas if $A(t) \le 1$, the rabbits switch to the exploitation phase, which is carried out via random hiding.

Proposed algorithm (DEARO)

The DEARO algorithm builds upon the standard ARO algorithm by introducing the following two changes, designed to enhance its search performance:

Following the principle that a mutation stage is essential for any meta-heuristic optimization algorithm [86], DEARO

Table 3 Comparison of estimated and measured values for I-V and P–V characteristics

Vcell	Icell	Vest	Pest	Pref	RE %	AE	MBE
29	0.6	28.99722	17.39833	17.4	0.009575	0.002777	4.28E−07
26.31	2.1	26.30594	55.24247	55.251	0.015443	0.004063	9.17E−07
25.09	3.58	25.09356	89.83493	89.8222	0.01417	0.003555	7.02E−07
24.25	5.08	24.25462	123.2135	123.19	0.019053	0.00462	1.19E−06
23.37	7.17	23.37542	167.6017	167.5629	0.023175	0.005416	1.63E−06
22.57	9.55	22.58461	215.6831	215.5435	0.064754	0.014615	1.19E−05
22.06	11.35	22.07133	250.5096	250.381	0.051348	0.011327	7.13E−06
21.75	12.54	21.75846	272.8511	272.745	0.038913	0.008463	3.98E−06
21.45	13.73	21.46126	294.6631	294.5085	0.052506	0.011263	7.05E−06
21.09	15.73	20.98774	330.1372	331.7457	0.484867	0.102258	0.000581
20.68	17.02	20.69451	352.2206	351.9736	0.070162	0.014509	1.17E−05
20.22	19.11	20.23099	386.6141	386.4042	0.054332	0.010986	6.71E−06
19.76	21.2	19.77094	419.144	418.912	0.055381	0.010943	6.65E−06
19.36	23	19.36602	445.4186	445.28	0.03112	0.006025	2.02E−06
18.86	25.08	18.86647	473.171	473.0088	0.034286	0.006466	2.32E−06
18.27	27.17	18.27472	496.5242	496.3959	0.025838	0.004721	1.24E−06
17.95	28.06	17.95331	503.7699	503.677	0.018444	0.003311	6.09E−07
17.3	29.26	17.29288	505.9896	506.198	0.041174	0.007123	2.82E−06
					0.061363	0.012913	3.61E−05

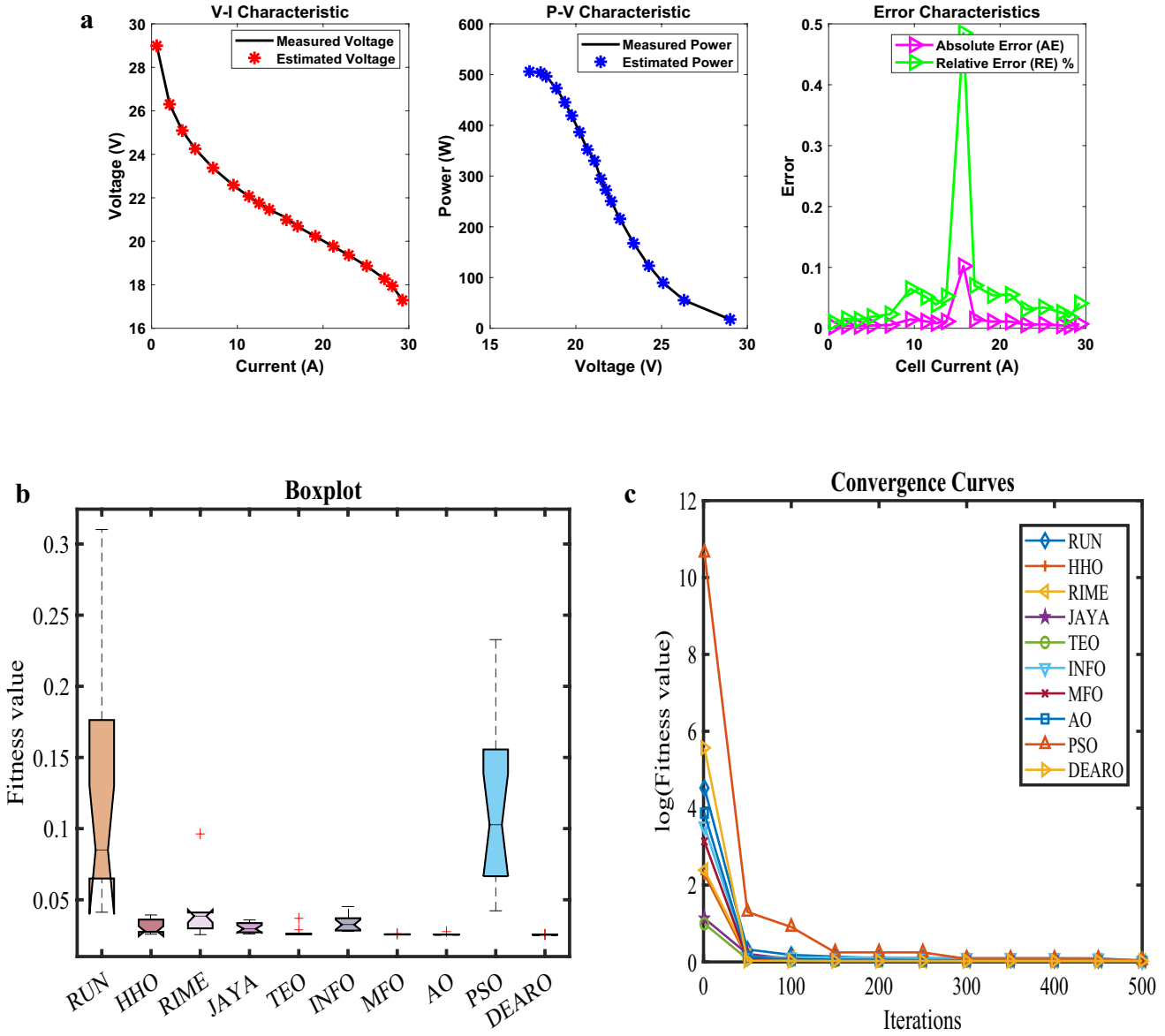

Fig. 2 **a** Graphical representation of I-V; P–V and error characteristics. **b** Box plot for error distribution across different algorithms. **c** Convergence curve showing optimization performance

includes this process to generate variants of current solutions within the search space, thereby preserving population diversity. To enhance the searching power of the ARO algorithm, the DEARO algorithm integrates the following three mutation strategies, inspired by the DE algorithm as represented in Eq. 38 to Eq. 40, in addition to its native Eqs. 28 and 33:

$$\vec{v}_i(t+1) = \vec{x}_{\text{best}}(t) + sf \otimes \left(\vec{x}_{r1}(t) - \vec{x}_{r2}(t) + \vec{x}_{r3}(t) - \vec{x}_{r4}(t)\right) \tag{38}$$

$$\vec{v}_i(t+1) = \vec{x}_{r1}(t) + sf \otimes \left(\vec{x}_{r2}(t) + \vec{x}_{r3}(t)\right) \tag{39}$$

$$\vec{v}_i(t+1) = \vec{x}_i(t) + \text{rand}(0,1) \otimes \left(\vec{x}_{r1}(t) - \vec{x}_i(t) + sf \otimes \left(\vec{x}_{r2}(t) + \vec{x}_{r3}(t)\right)\right) \tag{40}$$

where $\vec{x}_{\text{best}}(t)$ is the current best solution, sf is a random scale factor from SF, $\otimes$ is element-wise multiplication, and $\vec{x}_{r1-r4}(t)$ are four randomly and distinctly chosen solution vectors from the population at iteration t.

To enhance the performance of the basic ARO algorithm, DEARO employs a crossover operation. This operation, known for its ability to produce superior offspring by combining the best features of parent solutions, is particularly effective in complex and multi-modal optimization tasks [86]. Specifically, we have implemented binomial crossover to merge beneficial characteristics from different solutions. The binomial crossover mechanism allows each element of the new solution to be taken either

Table 4 Optimal parameter values and performance metrics

Algorithm	RUN	HHO	RIME	JAYA	TEO	INFO	MFO	AO	PSO	DEARO
ξ_1	−0.99447	−0.89272	−0.8532	−0.85835	−1.00422	−0.94579	−1.07692	−1.02444	−0.98029	−0.85617
ξ_2	0.002911	0.002573	0.002889	0.00311	0.003362	0.003537	0.003397	0.003109	0.002764	0.003132
ξ_3	4.32E−05	4.02E−05	7.11E−05	8.57E−05	7.34E−05	0.000098	6.07E−05	5.1E−05	0.000036	8.78E−05
ξ_4	−9.5E−05	−9.5E−05	−9.5E−05	−9.5E−05	−9.5E−05	−9.5E−05	−9.5E−05	−9.5E−05	−9.6E−05	−9.5E−05
λ	14.01541	14	14	14	14.0156	14	14	14.05153	14	14
R_c	0.0001	0.000123	0.0001	0.000126	0.00011	0.000125	0.000122	0.000121	0.0001	0.00012
B	0.020416	0.016494	0.019593	0.015939	0.018443	0.01633	0.016678	0.01759	0.018453	0.016788
Min	0.276815	0.275218	0.2759	0.275301	0.27598	0.275412	0.275224	0.275732	0.280841	0.275211
Max	1.44645	0.341011	0.336021	0.309874	0.299509	0.312033	0.296388	0.293236	0.540167	0.2759
Mean	0.563492	0.30209	0.2996	0.289318	0.284046	0.285734	0.277303	0.282137	0.349886	0.275256
Std	0.341246	0.021663	0.02633	0.01253	0.008184	0.012186	0.00533	0.004746	0.064184	0.000178
RT	13.08515	15.79815	12.94681	13.15416	28.37648	15.45895	14.54717	17.43564	28.67788	0.57674
FR	8.6	6.6	5.933333	5.466667	5.4	5.4	3.066667	4.733333	8.8	1

from the current solution vector or the mutant vector, as described in Eq. 41:

$$\vec{u}_i(t+1) = \begin{cases} \vec{v}_i(t)\, if\ rand\ < cr \\ \vec{x}_i(t) otherwise \end{cases} \tag{41}$$

Here, *cr* indicates the crossover rate, a value that determines the likelihood of a component being exchanged during the crossover operation.

The DEARO algorithm starts by creating an initial population of NP rabbits, where each rabbit represents a candidate solution. Each rabbit is assigned a randomly selected scale factor (sf) and crossover rate (cr) from predefined sets of SF and CR values. The algorithm then enters its main iterative loop to refine the solutions. Within this loop, mutation is performed on the rabbit population using Eqs. 28, 33 and 38 to 40 to generate new potential solutions. Subsequently, the crossover operation is applied to selected solutions ($\vec{v}_i(t)$) according to Eq. 41. Following the generation of new offspring, their positions are checked to ensure they remain within the defined search space. If an offspring falls outside these boundaries, it is replaced with a new, randomly generated solution within the valid range. The algorithm also incorporates a mechanism to learn and adapt its parameters: if a newly generated offspring exhibits better fitness than its randomly chosen parent, the associated *sf* and *cr* values are stored. Additionally, a 'failure' parameter tracks the number of times an offspring fails to improve upon its parent's fitness. At the end of each iteration, the average failure rate is calculated. If this rate is below a randomly generated number, previously stored *cr* and *sf* values are retrieved and used; otherwise, entirely new *cr* and *sf* values are randomly generated. The algorithm continues iterating until a termination criterion is met, at which point it returns the best solution found so far $\vec{x}_{\text{best}}(t)$.

Results analysis and discussion

Result analysis

To optimize the parameters of experimentally validated mathematical models representing various PEMFC stacks (BCS 500 W, Nedstack 600 W PS6, SR-12 W, Horizon H-12, Ballard Mark V and STD 250 W with their physical parameters in Table 1), the DEARO algorithm was computationally implemented. This implementation utilized MATLAB 2021a on a Windows Server 2019 system with an Intel Core i7-11700 k (3.6 GHz) processor and 32 GB RAM, ensuring efficient execution. The optimization problem was formulated to minimize the sum of squared errors (SSE) between experimental voltage readings and those predicted by the PEMFC models.

Table 5 Comparison of estimated and measured values for I-V and P–V characteristics

Vcell	Icell	Vest	Pest	Pref	RE %	AE	MBE
61.64	2.25	62.32708	140.2359	138.69	1.114671	0.687083	0.016279
59.57	6.75	59.75391	403.3389	402.0975	0.308722	0.183906	0.001166
58.94	9	59.02299	531.207	530.46	0.140813	0.082995	0.000238
57.54	15.75	57.47245	905.191	906.255	0.117401	0.067553	0.000157
56.8	20.25	56.69501	1148.074	1150.2	0.184848	0.104994	0.00038
56.13	24.75	56.02304	1386.57	1389.218	0.190562	0.106962	0.000395
55.23	31.5	55.13803	1736.848	1739.745	0.166516	0.091967	0.000292
54.66	36	54.60299	1965.708	1967.76	0.104294	0.057007	0.000112
53.61	45	53.61886	2412.849	2412.45	0.016533	0.008863	2.71E-06
52.86	51.75	52.93264	2739.264	2735.505	0.137426	0.072643	0.000182
51.91	67.5	51.43559	3471.902	3503.925	0.913916	0.474414	0.007761
51.22	72	51.02539	3673.828	3687.84	0.379942	0.194606	0.001306
49.66	90	49.42672	4448.405	4469.4	0.46976	0.233283	0.001877
49	99	48.64101	4815.46	4851	0.732639	0.358993	0.004444
48.15	105.8	48.04916	5083.601	5094.27	0.209422	0.100837	0.000351
47.52	110.3	47.6574	5256.611	5241.456	0.289134	0.137396	0.000651
47.1	117	47.07283	5507.521	5510.7	0.057687	0.02717	2.55E-05
46.48	126	46.28306	5831.665	5856.48	0.423715	0.196943	0.001337
45.66	135	45.4853	6140.516	6164.1	0.382603	0.174696	0.001052
44.85	141.8	44.87551	6363.347	6359.73	0.056876	0.025509	2.24E-05
44.24	150.8	44.05684	6643.772	6671.392	0.414008	0.183157	0.001157
42.45	162	43.01569	6968.542	6876.9	1.332607	0.565692	0.011035
41.66	171	42.15751	7208.934	7123.86	1.194214	0.49751	0.008535
40.68	182.3	41.04751	7482.96	7415.964	0.903407	0.367506	0.004657
40.09	189	40.36954	7629.843	7577.01	0.697275	0.279538	0.002695
39.51	195.8	39.66413	7766.236	7736.058	0.390097	0.154127	0.000819
38.73	204.8	38.69983	7925.726	7931.904	0.077892	0.030168	3.14E-05
38.15	211.5	37.95577	8027.646	8068.725	0.509117	0.194228	0.001301
37.38	220.5	36.91421	8139.583	8242.29	1.246095	0.46579	0.007481
					0.453869	0.211225	0.002612

The performance of the WAA algorithm was then rigorously evaluated by comparing its outcomes against a set of nine benchmark metaheuristic algorithms. To assess the DEARO algorithm, a comparative study was conducted against nine benchmark algorithms: RUN Algorithm (RUN), Harris Hawks Optimization (HHO), RIME Algorithm (RIME), JAYA Algorithm (JAYA), TEO Optimization (TEO), INFO Optimization (INFO), Moth Flame Optimizer (MFO), Aquila Optimizer (AO), and particle swarm optimization (PSO).

The success of the DEARO algorithm in the parameter extraction of PEMFC models is essentially based on the appropriate selection and optimization of the algorithm parameters, which were systematically calculated and validated by the thorough empirical analysis. The population size was set to 50 individuals following the comparative testing of alternative configurations (30, 70 and 100) because this value showed the best trade-off between the exploration ability and the computational efficiency of all 12 PEMFC case studies. Convergence analysis was used to determine the maximum number of iterations, which was set to 500 generations, as this value always enabled the algorithm to converge to stable solutions without premature stopping or an unreasonable amount of time.

In the case of mutation operation, DEARO uses an adaptive scale factor (SF) mechanism which dynamically picks values out of a predetermined pool [0.5, 0.6, 0.7, 0.8, 0.9, 1.0] depending on the past success rates. This strategy makes the algorithm diverse at the beginning of the optimization process and more local search at the end of the optimization process. Crossover rate (CR) is similar in its adaptive strategy, and values are sampled in [0.1, 0.2, 0.3,

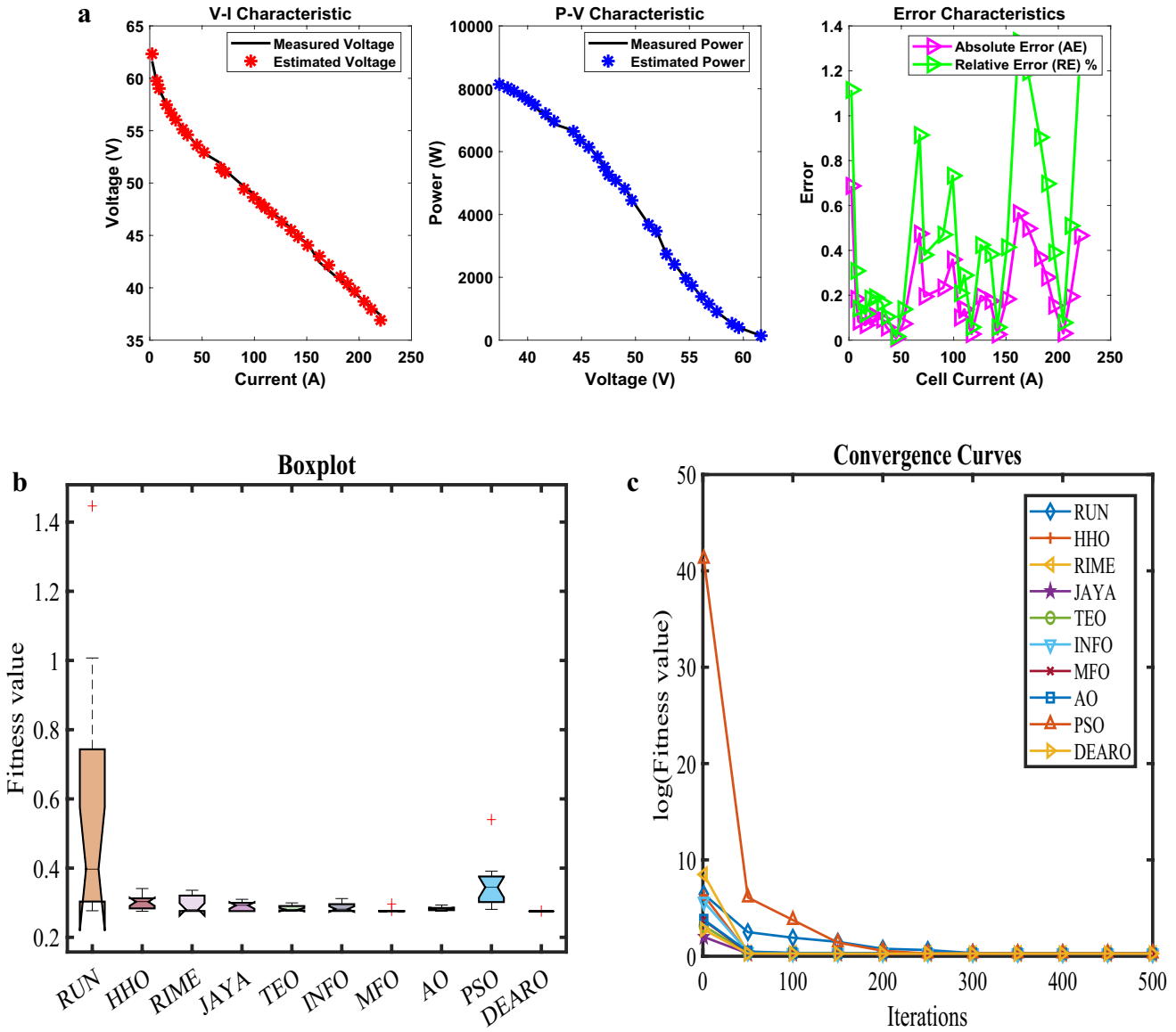

Fig. 3 **a** Graphical representation of I-V; P–V and error characteristics. **b** Box plot for error distribution across different algorithms. **c** Convergence curve showing optimization performance

0.4, 0.5, 0.6, 0.7, 0.8, 0.9] and updated based on a failure-rate measure, which keeps track of the progress of candidate solutions. When the failure rate is above a dynamically changing threshold, the algorithm will use previously successful CR and SF values; otherwise, random new values are chosen to promote exploration.

Also, DEARO uses a binomial crossover method to improve the quality of solutions by combining the favourable characteristics of parent vectors. This selection pressure is regulated by a greedy replacement strategy, in which offspring solutions only replace their parents when they are fitter, which guarantees monotonic improvement of solution quality. The results of these parameter settings were highly reproducible with a low variance as shown by the low standard deviations in the fitness values obtained in multiple independent runs. The robustness of the algorithm is also reflected by its fast convergence, which usually finds near-optimal solutions in the first 50–100 iterations, thus saving a lot of computational cost and at the same time ensuring high accuracy in parameter estimation. The combination of these design decisions makes DEARO outperform in PEMFC modelling applications. These design decisions

Table 6 Optimal parameter values and performance metrics

Algorithm	RUN	HHO	RIME	JAYA	TEO	INFO	MFO	AO	PSO	DEARO
ξ_1	−1.08062	−0.86031	−0.8532	−1.14636	−1.02053	−1.02542	−1.0807	−1.09467	−1.0047	−1.19969
ξ_2	0.003644	0.002802	0.003127	0.003787	0.003325	0.003633	0.003065	0.003229	0.002792	0.004148
ξ_3	7.8E−05	6.78E−05	9.02E−05	7.42E−05	6.95E−05	8.84E−05	4.07E−05	4.85E−05	3.84E−05	8.68E−05
ξ_4	−9.5E−05	−9.6E−05	−9.5E−05	−9.6E−05	−9.5E−05	−9.5E−05	−9.5E−05	−9.5E−05	−9.7E−05	−9.5E−05
λ	19.20336	22.16463	23	17.54377	22.95363	23	22.999	22.97046	14.6255	23
R_c	0.0008	0.000609	0.000673	0.000506	0.000691	0.000711	0.000673	0.000668	0.000369	0.000673
B	0.171126	0.176222	0.17532	0.176483	0.174905	0.174508	0.175269	0.175465	0.177537	0.17532
Min	0.243854	0.242434	0.242284	0.242881	0.242305	0.242335	0.242312	0.24229	0.248966	0.242284
Max	0.943461	0.250067	0.247458	0.246488	0.243199	0.250006	0.242519	0.24255	0.728392	0.242927
Mean	0.520035	0.244557	0.24436	0.244727	0.242712	0.245758	0.24239	0.24239	0.448575	0.242433
Std	0.242043	0.002172	0.001886	0.00114	0.000296	0.002407	5.37E−05	8.67E−05	0.159738	0.000268
RT	8.203922	10.40486	8.861373	9.763495	20.70437	11.15235	10.58489	13.30653	22.99467	0.369199
FR	9.4	6.066667	5.2	6.6	4.066667	6.8	2.666667	2.733333	9.4	2.066667

make DEARO outperform in PEMFC modelling applications. The convergence properties of the algorithm were also examined graphically, such as box plots and fitness progression plots, which proved that the algorithm converged quickly and steadily in all PEMFC test cases. All these implementation decisions lead to the DEARO having high accuracy in parameter estimation and still being computationally efficient.

The evaluation of DEARO focused on its convergence behaviour, error distribution patterns and stability when modelling different PEMFC stacks. The quantitative discrepancy between estimated and real voltage values was determined using absolute error (AE), relative error (RE) and mean bias error (MBE). The performance analysis was supported by graphical representations such as I–V and P–V curves, box plots and convergence curves. Friedman ranking tests confirmed the statistical significance of DEARO's enhanced results compared to existing approaches. Recent studies have advanced PEMFC parameter estimation techniques, including machine learning approaches [87], as well as integrated reviews of fuel cell–based hybrid electric vehicles [88]. Additionally, challenges in multi-stack systems [89] and co-optimization strategies for fuel cell durability [90] have been explored. A thorough analysis of these results then demonstrated DEARO's capability for optimal PEMFC parameter optimization, highlighting its computational effectiveness and robust design characteristics.

The experimental section has been expanded to include detailed specifications for each of the 12 PEMFC systems, as presented in Table 1. This table comprehensively lists critical parameters such as PEMFC type, power output (W), number of cells (Ncells), membrane active area (cm^2), membrane thickness (μm), operating temperature (K), maximum current density (mA/cm^2) and partial pressures of hydrogen (PH_2) and oxygen (PO_2) in bar. For instance, the BCS 500 W stack comprises 32 cells with an active area of 64 cm^2, operating at 333 K, while the NedStack PS6 system features 65 cells with a 240 cm^2 active area at 343 K. These specifications provide essential context for understanding the diverse operating conditions and design configurations under which the DEARO algorithm was validated. The inclusion of such granular details ensures reproducibility and facilitates a more rigorous evaluation of the algorithm's performance across varying PEMFC architectures and operational regimes. The additional system parameters enable readers to better assess the applicability of the proposed method to different PEMFC configurations. For example, the Horizon H-12 stacks (H-12–1, H-12–2, H-12–3) exhibit progressively lower operating temperatures (323 K, 302 K, 312 K), allowing for analysis of temperature-dependent parameter sensitivity. Similarly, the STD series (STD-1 to STD-4) demonstrates variations in hydrogen pressure

Table 7 Comparison of estimated and measured values for I-V and P–V characteristics

Vcell	Icell	Vest	Pest	Pref	RE %	AE	MBE
43.17	1.004	43.34081	43.51417	43.34268	0.395667	0.170809	0.001621
41.14	3.166	41.09008	130.0912	130.2492	0.121347	0.049922	0.000138
40.09	5.019	39.91451	200.3309	201.2117	0.437735	0.175488	0.001711
39.04	7.027	38.85715	273.0492	274.3341	0.46836	0.182848	0.001857
37.99	8.958	37.93346	339.808	340.3144	0.148816	0.056535	0.000178
37.08	10.97	37.01454	406.0495	406.7676	0.176546	0.065463	0.000238
36.03	13.05	36.07991	470.8428	470.1915	0.138511	0.049906	0.000138
35.19	15.06	35.17136	529.6807	529.9614	0.052958	0.018636	1.93E-05
34.07	17.07	34.24209	584.5124	581.5749	0.505102	0.172088	0.001645
33.02	19.07	33.28313	634.7092	629.6914	0.796869	0.263126	0.003846
32.04	21.08	32.2707	680.2664	675.4032	0.720038	0.2307	0.002957
31.2	23.01	31.23769	718.7793	717.912	0.120813	0.037694	7.89E-05
29.8	24.94	30.12737	751.3766	743.212	1.098562	0.327372	0.005954
28.96	26.87	28.91713	777.0034	778.1552	0.148018	0.042866	0.000102
28.12	28.96	27.45776	795.1766	814.3552	2.355061	0.662243	0.024365
26.3	30.81	25.9918	800.8075	810.303	1.171846	0.308195	0.005277
24.06	32.97	23.98487	790.7811	793.2582	0.312265	0.075131	0.000314
21.4	34.9	21.78563	760.3186	746.86	1.802028	0.385634	0.008262
					0.609475	0.181925	0.003261

(1.0–2.5 bar) and membrane thickness (127 µm vs. 25 µm in other stacks), highlighting the algorithm's robustness under differing mass transport conditions. Such detailed characterization of test systems is crucial for interpreting the convergence behaviour and accuracy of parameter estimation, particularly when comparing results across stacks with differing scales, materials or operating regimes.

Sheet 1: BCS 500 W

The DEARO algorithm was used to optimize the parameters of the BCS 500 W PEMFC stack, and its performance was benchmarked against nine other algorithms: RUN, HHO, RIME, JAYA, TEO, INFO, MFO, AO and PSO. Table 2 highlights DEARO's effectiveness in achieving the minimum fitness value (0.025493) and its superior stability, evidenced by the lowest standard deviation (5.91E − 05). Notably, DEARO also demonstrated the fastest computational time (0.386165 s), making it well-suited for real-time and computationally limited settings. The Friedman rank analysis further confirmed DEARO's overall superior performance, assigning it the top rank of (1.2). Conversely, the MFO and AO algorithms displayed higher variability in their results, which could impact their dependability in parameter estimation.

As part of the validation process, the correlation between actual measured data and power across varying cell currents was examined, with the findings presented in Table 3. The model's high estimation accuracy is supported by an average absolute error of 0.012913 and a percentage relative error of 0.061363%, indicating that DEARO effectively captures the fuel cell's operational behaviour. Furthermore, the validation showed minimal systematic bias, with a mean bias error of 3.61E − 05.

The experimental findings depicted in Fig. 2a, b, c provide strong visual evidence of DEARO's robustness. Figure 2a V-I and P–V curves show a strong correlation between experimental data and the model's predictions, illustrating its accurate operation across a spectrum of conditions. The error characteristics plot visually confirms the reliability of DEARO's predictions, as absolute and relative errors remain consistently low. Furthermore, the boxplot in Fig. 2b visually highlights DEARO's high stability through its compact interquartile range and minimal outliers, in stark contrast to the considerable performance fluctuations observed in other algorithms. Figure 2 c visually showcases DEARO's speed in reaching the optimal fitness, achieving the desired result within the initial 50 iterations, in contrast to the slower or inconsistent convergence of other optimization methods. The BCS 500 W PEMFC case study results establish DEARO's highly accurate and stable parameter optimization capabilities. DEARO's efficiency in quickly locating optimal solutions while demanding minimal computational resources underscores its advantage as a parameter estimation method for PEMFCs, outperforming conventional approaches.

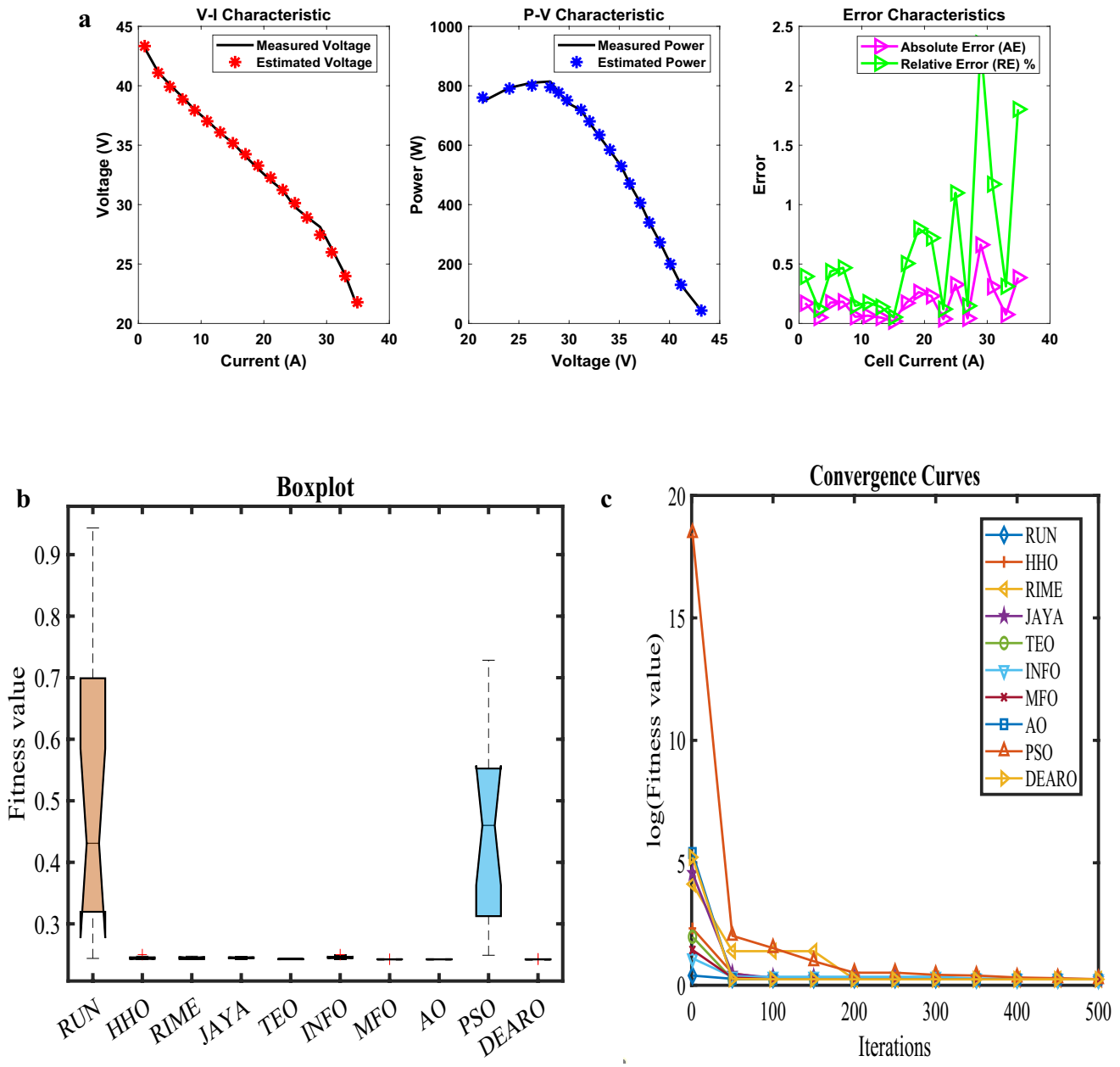

Fig. 4 **a** Graphical representation of I-V; P–V and error characteristics. **b** Box plot for error distribution across different algorithms, **c** Convergence curve showing optimization performance

Sheet 2: NetStack PS6

The DEARO algorithm was used to optimize the parameters of the NetStack PS6 PEMFC stack, and its performance was benchmarked against nine other algorithms: RUN, HHO, RIME, JAYA, TEO, INFO, MFO, AO and PSO. Table 4 highlights DEARO's effectiveness in achieving the minimum fitness value (0.275211) and its superior stability, evidenced by the lowest standard deviation (0.000178). Notably, DEARO also demonstrated the fastest computational time (0.57674 s), making it well-suited for real-time and computationally limited settings. The Friedman rank analysis further confirmed DEARO's overall superior performance, assigning it the top rank of (1). Conversely, the MFO and AO algorithms displayed higher variability in their results, which could impact their dependability in parameter estimation.

As part of the validation process, the correlation between actual measured data and power across varying cell currents

Table 8 Optimal parameter values and performance metrics

Algorithm	RUN	HHO	RIME	JAYA	TEO	INFO	MFO	AO	PSO	DEARO
ξ_1	−0.86827	−0.8532	−1.19969	−1.03806	−0.99496	−1.19462	−1.12734	−1.17599	−0.97064	−0.8532
ξ_2	0.002128	0.001509	0.00333	0.002109	0.002421	0.00299	0.002793	0.002598	0.001953	0.001509
ξ_3	7.72E−05	3.6E−05	8.98E−05	3.8E−05	7E−05	6.65E−05	6.73E−05	4.24E−05	4.2E−05	0.000036
ξ_4	−0.00011	−0.00011	−0.00011	−0.00011	−0.00011	−0.00011	−0.00011	−0.00011	−0.00011	−0.00011
λ	14	14	14	14.02318	14.00041	14.04588	14	14.00433	14	14
R_c	0.0008	0.0008	0.0008	0.000758	0.0008	0.000585	0.0008	0.0008	0.000168	0.0008
B	0.0136	0.0136	0.0136	0.013608	0.013601	0.013661	0.0136	0.0136	0.0136	0.0136
Min	0.102915	0.102915	0.102915	0.102975	0.102915	0.103158	0.102915	0.102917	0.10362	0.102915
Max	0.118954	0.103658	0.105211	0.105257	0.103408	0.105149	0.108683	0.102942	0.112051	0.103641
Mean	0.107248	0.103355	0.103818	0.103769	0.103032	0.103947	0.1033	0.102923	0.106495	0.102963
Std	0.005434	0.000305	0.000827	0.000641	0.000149	0.000596	0.001489	6.56E−06	0.002553	0.000187
RT	7.572452	9.861563	9.944478	9.047766	20.22648	10.97038	12.48219	12.89669	20.40192	0.402319
FR	7	5.533333	6.066667	6.733333	4.666667	7.333333	3.133333	4.066667	8.933333	1.533333

Table 9 Comparison of estimated and measured values for I-V and P–V characteristics

Vcell	Icell	Vest	Pest	Pref	RE %	AE	MBE
9.58	0.104	9.755532	1.014575	0.99632	1.832272	0.175532	0.001712
9.42	0.2	9.435534	1.887107	1.884	0.164909	0.015534	1.34E−05
9.25	0.309	9.215306	2.84753	2.85825	0.37507	0.034694	6.69E−05
9.2	0.403	9.075995	3.657626	3.7076	1.347879	0.124005	0.000854
9.09	0.51	8.947893	4.563425	4.6359	1.563338	0.142107	0.001122
8.95	0.614	8.842715	5.429427	5.4953	1.19872	0.107285	0.000639
8.85	0.703	8.762861	6.160291	6.22155	0.984618	0.087139	0.000422
8.74	0.806	8.678685	6.99502	7.04444	0.70154	0.061315	0.000209
8.65	0.908	8.601587	7.810241	7.8542	0.559683	0.048413	0.00013
8.45	1.076	8.483394	9.128131	9.0922	0.39519	0.033394	6.2E−05
8.41	1.127	8.448867	9.521873	9.47807	0.462156	0.038867	8.39E−05
8.2	1.288	8.341384	10.7437	10.5616	1.724194	0.141384	0.001111
8.12	1.39	8.272663	11.499	11.2868	1.880081	0.152663	0.001295
8.11	1.45	8.231198	11.93524	11.7595	1.494432	0.121198	0.000816
8.05	1.578	8.137515	12.841	12.7029	1.087138	0.087515	0.000425
7.99	1.707	8.028856	13.70526	13.63893	0.486306	0.038856	8.39E−05
7.95	1.815	7.912602	14.36137	14.42925	0.47041	0.037398	7.77E−05
7.94	1.9	7.777413	14.77708	15.086	2.047696	0.162587	0.001469
					1.043091	0.089438	0.000588

was examined, with the findings presented in Table 5. The model's high estimation accuracy is supported by an average absolute error of 0.211225 and a percentage relative error of 0.002612%, indicating that DEARO effectively captures the fuel cell's operational behaviour. Furthermore, the validation showed minimal systematic bias, with a mean bias error of 3.61E−05.

The experimental findings depicted in Fig. 3a, b, c provide strong visual evidence of DEARO's robustness. Figure 3 a V-I and P–V curves show a strong correlation between experimental data and the model's predictions, illustrating its accurate operation across a spectrum of conditions. The error characteristics plot visually confirms the reliability of DEARO's predictions, as absolute and relative errors remain consistently low. Furthermore, the boxplot in Fig. 3b visually highlights DEARO's high stability through its compact interquartile range and minimal outliers, in stark contrast to the considerable performance fluctuations observed in other algorithms. Figure 3 c visually showcases DEARO's speed

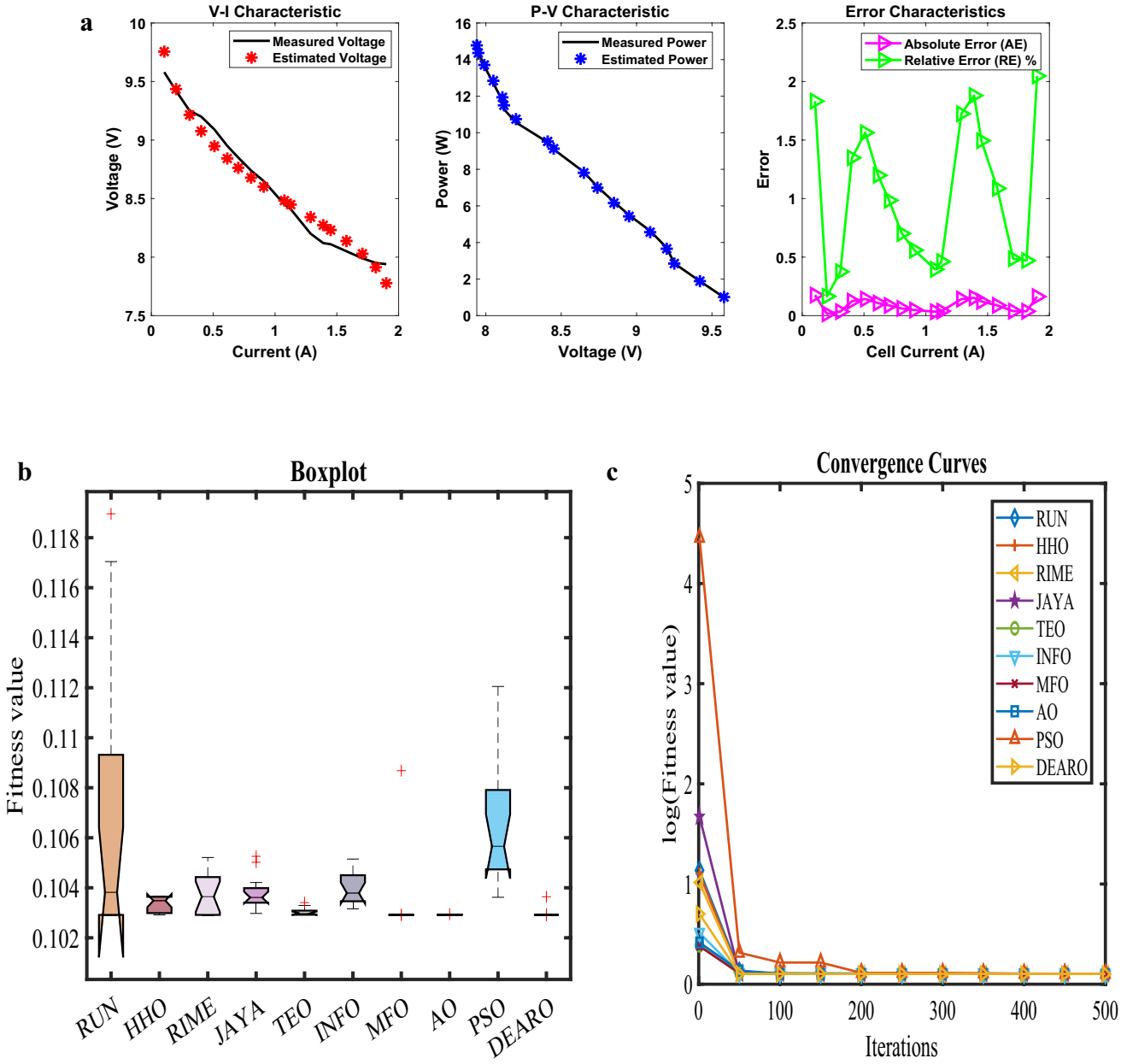

Fig. 5 **a** Graphical representation of I-V; P–V and error characteristics. **b** Box plot for error distribution across different algorithms. **c** Convergence curve showing optimization performance

in reaching the optimal fitness, achieving the desired result within the initial 50 iterations, in contrast to the slower or inconsistent convergence of other optimization methods. The NetStack PS6 PEMFC case study results establish DEARO's highly accurate and stable parameter optimization capabilities. DEARO's efficiency in quickly locating optimal solutions while demanding minimal computational resources underscores its advantage as a parameter estimation method for PEMFCs, outperforming conventional approaches.

Sheet 3: SR-12

The DEARO algorithm was used to optimize the parameters of the SR-12 PEMFC stack, and its performance was benchmarked against nine other algorithms: RUN, HHO, RIME, JAYA, TEO, INFO, MFO, AO and PSO. Table 6 highlights DEARO's effectiveness in achieving the minimum fitness value (0.242284) and its superior stability, evidenced by the lowest standard deviation (0.000268). Notably, DEARO also demonstrated the fastest computational time (0.369199 s),

Table 10 Optimal parameter values and performance metrics

Algorithm	RUN	HHO	RIME	JAYA	TEO	INFO	MFO	AO	PSO	DEARO
ξ_1	−0.85586	−1.05373	−1.19969	−0.87022	−1.12298	−0.85671	−1.00246	−0.96591	−0.93797	−0.85336
ξ_2	0.002443	0.003045	0.004138	0.002828	0.003451	0.002725	0.003137	0.00326	0.002522	0.002548
ξ_3	4.87E−05	5.04E−05	0.000098	7.31E−05	6.49E−05	6.84E−05	6.76E−05	8.4E−05	3.71E−05	5.66E−05
ξ_4	−0.00017	−0.00017	−0.00017	−0.00017	−0.00017	−0.00018	−0.00017	−0.00017	−0.00017	−0.00017
λ	14.90955	14.53208	14.43913	14.56559	14.45123	14.84488	14.51131	14.42014	14.74781	14.43913
R_c	0.000379	0.000206	0.0001	0.000202	0.000102	0.000149	0.0001	0.000101	0.000276	0.0001
B	0.013745	0.013602	0.013795	0.013735	0.013813	0.014215	0.01389	0.013744	0.014028	0.013795
Min	0.149237	0.148824	0.148632	0.148842	0.148635	0.148858	0.148643	0.148634	0.149296	0.148632
Max	0.222436	0.157421	0.161938	0.152396	0.150264	0.152604	0.148806	0.149171	0.237572	0.148634
Mean	0.174716	0.151367	0.149836	0.149764	0.149142	0.150184	0.1487	0.148746	0.167648	0.148632
Std	0.020996	0.002552	0.003377	0.001164	0.000494	0.001243	4.95E−05	0.000146	0.025219	5.55E−07
RT	6.704361	8.829429	7.443644	6.384928	12.46586	7.315126	6.858657	8.706913	13.30018	0.323328
FR	9.4	7	3.933333	6.533333	5.2	6.6	3	3.466667	8.733333	1.133333

Table 11 Comparison of estimated and measured values for I-V and P–V characteristics

Vcell	Icell	Vest	Pest	Pref	RE %	AE	MBE
23.5	0.5	23.48309	11.74154	11.75	0.071975	0.016914	1.91E−05
21.5	2.1	21.2513	44.62774	45.15	1.156727	0.248696	0.004123
20.5	2.8	20.75981	58.12748	57.4	1.267389	0.259815	0.0045
19.9	4	20.10958	80.43831	79.6	1.053152	0.209577	0.002928
19.5	5.7	19.39753	110.5659	111.15	0.525477	0.102468	0.0007
19	7.1	18.90725	134.2415	134.9	0.488139	0.092746	0.000573
18.5	8	18.61964	148.9571	148	0.646705	0.11964	0.000954
17.8	11.1	17.72275	196.7226	197.58	0.433969	0.077246	0.000398
17.3	13.7	17.02409	233.23	237.01	1.594863	0.275911	0.005075
16.2	16.5	16.27464	268.5316	267.3	0.460763	0.074644	0.000371
15.9	17.5	15.99828	279.9699	278.25	0.618116	0.09828	0.000644
15.5	18.9	15.59366	294.7201	292.95	0.604245	0.093658	0.000585
15.1	20.3	15.15114	307.5681	306.53	0.338674	0.05114	0.000174
14.6	22	14.47819	318.5201	321.2	0.834336	0.121813	0.000989
13.8	22.9	13.82904	316.685	316.02	0.210444	0.029041	5.62E−05
					0.686998	0.124773	0.001473

making it well-suited for real-time and computationally limited settings. The Friedman rank analysis further confirmed DEARO's overall superior performance, assigning it the top rank of 2.066667. Conversely, the MFO and AO algorithms displayed higher variability in their results, which could impact their dependability in parameter estimation.

As part of the validation process, the correlation between actual measured data and power across varying cell currents was examined, with the findings presented in Table 7. The model's high estimation accuracy is supported by an average absolute error of 0.181925 and a percentage relative error of 0.609475%, indicating that DEARO effectively captures the fuel cell's operational behaviour. Furthermore, the validation showed minimal systematic bias, with a mean bias error of 0.003261.

The experimental findings depicted in Fig. 4 a, b, c provide strong visual evidence of DEARO's robustness. Figure 4 a V-I and P–V curves show a strong correlation between experimental data and the model's predictions, illustrating its accurate operation across a spectrum of conditions. The error characteristics plot visually confirms the reliability of DEARO's predictions, as absolute and relative errors remain consistently low. Furthermore, the boxplot in Fig. 4b visually highlights DEARO's high stability through its compact interquartile range and minimal outliers, in stark contrast to the considerable performance

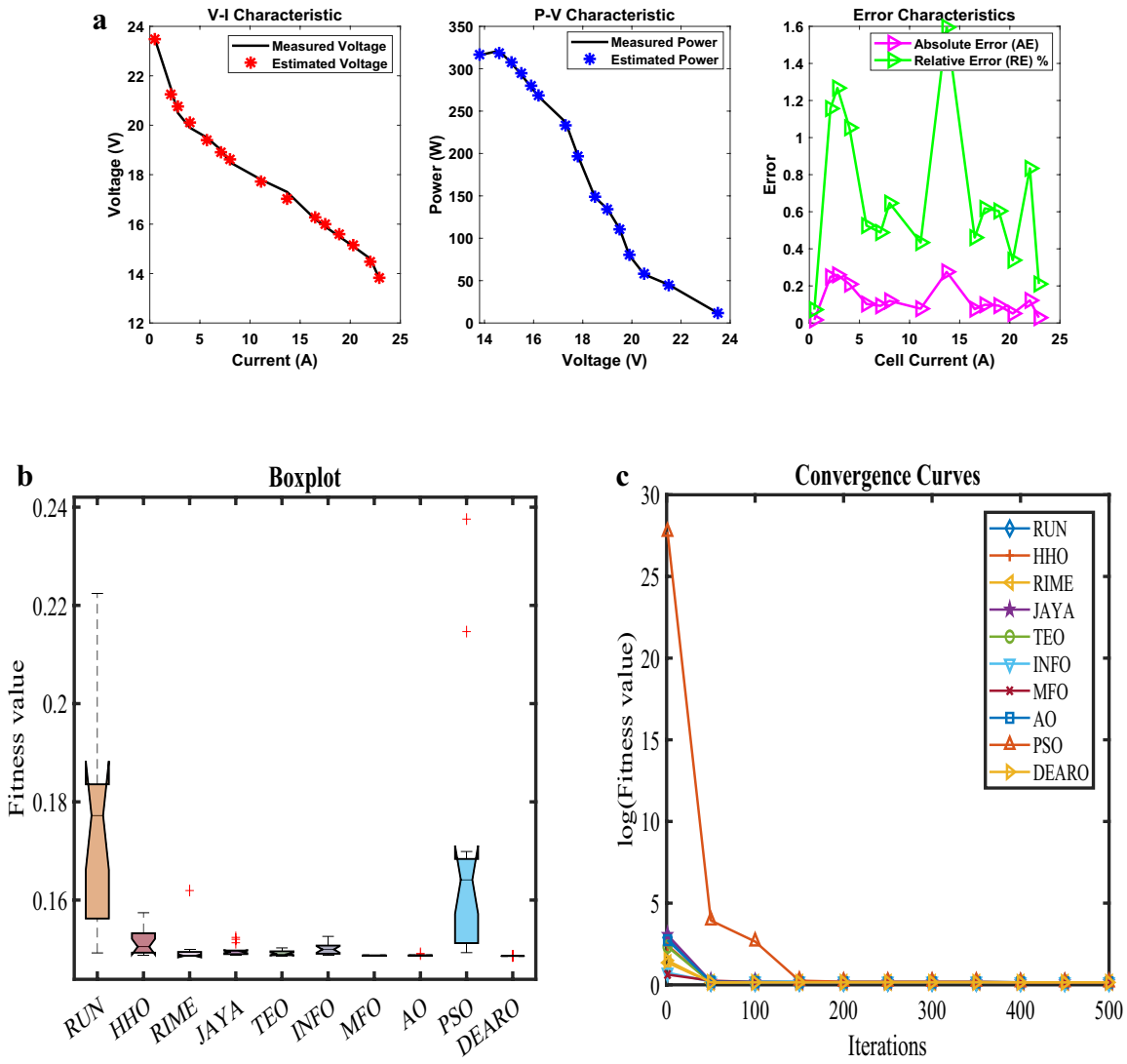

Fig. 6 **a** Graphical representation of I-V; P–V and error characteristics. **b** Box plot for error distribution across different algorithms. **c** Convergence curve showing optimization performance

Table 12 Optimal parameter values and performance metrics

Algorithm	RUN	HHO	RIME	JAYA	TEO	INFO	MFO	AO	PSO	DEARO
ξ_1	−0.8532	−1.19915	−1.19969	−0.87612	−0.89675	−1.11873	−1.11011	−1.02976	−1.07659	−0.85347
ξ_2	0.00209	0.003353	0.003536	0.002565	0.002632	0.003086	0.002993	0.003047	0.002694	0.001897
ξ_3	5.18E−05	6.83E−05	8.13E−05	8.03E−05	8.08E−05	6.61E−05	6.14E−05	8.23E−05	4.77E−05	3.74E−05
ξ_4	−0.00017	−0.00017	−0.00017	−0.00017	−0.00017	−0.00017	−0.00017	−0.00017	−0.00017	−0.00017
λ	14	14	14	14.00883	14	14.23874	14	14.00026	14.03712	14
R_c	0.0008	0.0008	0.0008	0.0008	0.0008	0.0008	0.0008	0.0008	0.000782	0.0008
B	0.017531	0.017318	0.017317	0.017299	0.017317	0.016921	0.017332	0.017325	0.01672	0.017317
Min	0.286779	0.283774	0.283774	0.283815	0.283774	0.284857	0.283777	0.283775	0.289878	0.283774
Max	0.483066	0.328309	0.382995	0.334544	0.285956	0.33766	0.283933	0.283889	0.416695	0.283774
Mean	0.359775	0.292986	0.305035	0.31182	0.283981	0.311113	0.283814	0.283812	0.340603	0.283774
Std	0.065937	0.014647	0.032471	0.017903	0.000573	0.018931	4.62E−05	3.63E−05	0.035724	3.85E−16
RT	6.116629	6.083758	5.420631	5.649275	11.57893	6.703329	6.364188	8.214718	12.36892	0.332803
FR	8.533333	4.666667	5.066667	7.266667	3.8	7.666667	4.066667	4.066667	8.8	1.066667

Table 13 Comparison of estimated and measured values for I-V and P–V characteristics

Vcell	Icell	Vest	Pest	Pref	RE %	AE	MBE
29.37	0.6	29.7147	17.82882	17.622	1.17364	0.344698	0.00914
26.77739	2.5	26.62879	66.57198	66.94348	0.554931	0.148596	0.001699
25.29025	5	25.00559	125.0279	126.4513	1.125585	0.284663	0.006233
24.28186	7.5	23.96352	179.7264	182.1139	1.311014	0.318339	0.007795
23.418	10	23.14754	231.4754	234.18	1.154903	0.270455	0.005627
22.7391	12	22.57673	270.9208	272.8692	0.714072	0.162374	0.002028
22.05852	14	22.04306	308.6028	308.8193	0.070117	0.015467	1.84E − 05
21.38615	16	21.52088	344.3341	342.1784	0.630007	0.134734	0.001396
20.72173	18	20.98016	377.6428	372.9911	1.247139	0.258429	0.005137
20.026	20	20.364	407.28	400.52	1.687803	0.337999	0.008788
19.63635	21	19.98091	419.5992	412.3634	1.75473	0.344565	0.009133
19.19181	22	19.45678	428.0492	422.2198	1.380673	0.264976	0.005401
18.66363	23	18.17812	418.0968	429.2635	2.60136	0.485508	0.018132
					1.185075	0.259293	0.006194

fluctuations observed in other algorithms. Figure 4 c visually showcases DEARO's speed in reaching the optimal fitness, achieving the desired result within the initial 50 iterations, in contrast to the slower or inconsistent convergence of other optimization methods. The SR-12 PEMFC case study results establish DEARO's highly accurate and stable parameter optimization capabilities. DEARO's efficiency in quickly locating optimal solutions while demanding minimal computational resources underscores its advantage as a parameter estimation method for PEMFCs, outperforming conventional approaches.

Sheet 4: H-12–1

The DEARO algorithm was used to optimize the parameters of the H-12–1 PEMFC stack, and its performance was benchmarked against nine other algorithms: RUN, HHO, RIME, JAYA, TEO, INFO, MFO, AO and PSO. Table 8 highlights DEARO's effectiveness in achieving the minimum fitness value (0.102915) and its superior stability, evidenced by the lowest standard deviation (0.000187). Notably, DEARO also demonstrated the fastest computational time (0.402319 s), making it well-suited for real-time and computationally limited settings. The Friedman rank analysis further confirmed DEARO's overall superior performance, assigning it the top rank of 1.533333. Conversely, the MFO and AO algorithms displayed higher variability in their results, which could impact their dependability in parameter estimation.

As part of the validation process, the correlation between actual measured data and power across varying cell currents was examined, with the findings presented in Table 9. The model's high estimation accuracy is supported by an average absolute error of 0.089438 and a percentage relative error of 1.043091%, indicating that DEARO effectively captures the fuel cell's operational behaviour. Furthermore, the validation showed minimal systematic bias, with a mean bias error of 0.000588.

The experimental findings depicted in Fig. 5a, b, c provide strong visual evidence of DEARO's robustness. Figure 5 a V-I and P–V curves show a strong correlation between experimental data and the model's predictions, illustrating its accurate operation across a spectrum of conditions. The error characteristics plot visually confirms the reliability of DEARO's predictions, as absolute and relative errors remain consistently low. Furthermore, the boxplot in Fig. 5b visually highlights DEARO's high stability through its compact interquartile range and minimal outliers, in stark contrast to the considerable performance fluctuations observed in other algorithms. Figure 5 c visually showcases DEARO's speed in reaching the optimal fitness, achieving the desired result within the initial 50 iterations, in contrast to the slower or inconsistent convergence of other optimization methods. The H-12–1 PEMFC case study results establish DEARO's highly accurate and stable parameter optimization capabilities. DEARO's efficiency in quickly locating optimal solutions while demanding minimal computational resources underscores its advantage as a parameter estimation method for PEMFCs, outperforming conventional approaches.

Sheet 5: Ballard Mark V

The DEARO algorithm was used to optimize the parameters of the Ballard Mark V PEMFC stack, and its performance was benchmarked against nine other algorithms: RUN,

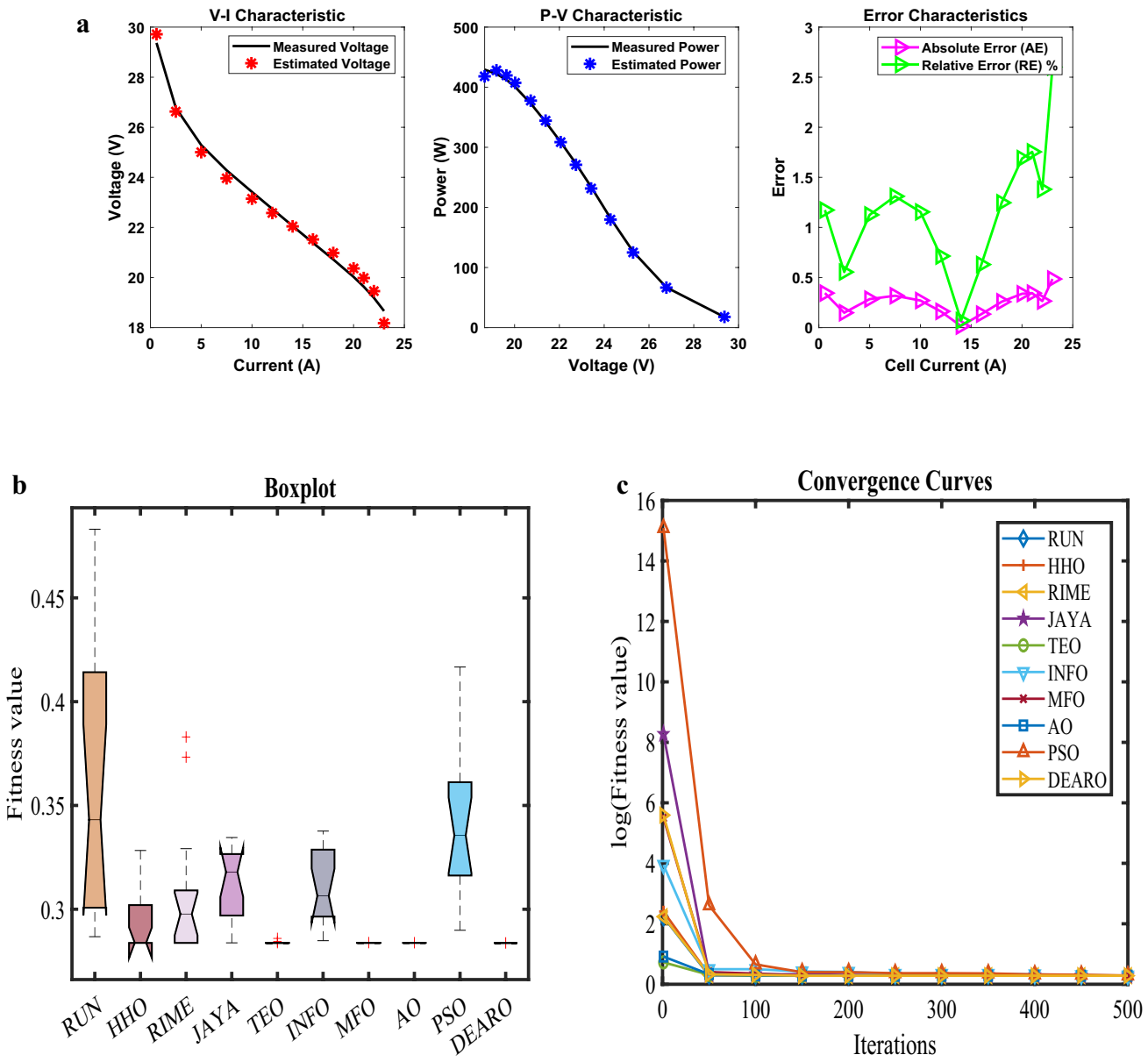

Fig. 7 **a** Graphical representation of I-V, P–V and error characteristics. **b** Box plot for error distribution across different algorithms. **c** Convergence curve showing optimization performance

HHO, RIME, JAYA, TEO, INFO, MFO, AO and PSO. Table 10 highlights DEARO's effectiveness in achieving the minimum fitness value (0.148632) and its superior stability, evidenced by the lowest standard deviation (5.55E − 07). Notably, DEARO also demonstrated the fastest computational time (0.323328 s), making it well-suited for real-time and computationally limited settings. The Friedman rank analysis further confirmed DEARO's overall superior performance, assigning it the top rank of 1.133333. Conversely, the MFO and AO algorithms displayed higher variability in their results, which could impact their dependability in parameter estimation.

As part of the validation process, the correlation between actual measured data and power across varying cell currents was examined, with the findings presented in Table 11. The model's high estimation accuracy is supported by an average absolute error of 0.124773 and a percentage relative error of 0.686998%, indicating that DEARO effectively captures the fuel cell's operational behaviour. Furthermore, the validation showed minimal systematic bias, with a mean bias error of 0.001473.

Table 14 Optimal parameter values and performance metrics

Algorithm	RUN	HHO	RIME	JAYA	TEO	INFO	MFO	AO	PSO	DEARO
ξ_1	−1.09336	−1.01122	−1.15194	−1.00546	−1.02326	−0.88759	−0.93687	−1.17282	−0.8632	−1.19969
ξ_2	0.002825	0.002814	0.003726	0.002686	0.002558	0.002354	0.00267	0.003532	0.002385	0.003643
ξ_3	4.48E−05	6.11E−05	0.000098	5.3E−05	3.97E−05	5.4E−05	6.65E−05	7.92E−05	6.1E−05	8.16E−05
ξ_4	−0.00014	−0.00015	−0.00015	−0.00015	−0.00015	−0.00015	−0.00015	−0.00015	−0.00015	−0.00015
λ	23	22.99987	23	22.89791	22.99999	22.53365	23	22.99986	22.1041	23
R_c	0.00014	0.0001	0.0001	0.000106	0.0001	0.000133	0.0001	0.0001	0.000166	0.0001
B	0.052778	0.051001	0.050979	0.051016	0.050982	0.05119	0.050974	0.050984	0.050811	0.050979
Min	0.131022	0.121756	0.121755	0.12214	0.121755	0.124402	0.121778	0.12176	0.126071	0.121755
Max	0.242162	0.145991	0.160077	0.132036	0.122608	0.146808	0.122384	0.121999	0.423123	0.121755
Mean	0.152961	0.128987	0.132302	0.12644	0.121967	0.132543	0.121948	0.121802	0.229506	0.121755
Std	0.028682	0.006563	0.01142	0.003529	0.000253	0.006816	0.000194	6.1E−05	0.086977	1.25E−16
RT	6.800897	6.59143	5.715846	6.154573	12.75394	7.522052	6.939594	12.41779	22.50068	1.088311
FR	8.6	6.533333	5.4	6	3.4	7.266667	3.933333	3.2	9.666667	1

Table 15 Comparison of estimated and measured values for I-V and P–V characteristics

Vcell	Icell	Vest	Pest	Pref	RE %	AE	MBE
22.6916	0.2417	22.56459	5.453861	5.48456	0.559736	0.127013	0.001075
20.1869	1.3177	20.35845	26.82634	26.60028	0.849833	0.171555	0.001962
19.2897	2.6819	19.32465	51.82677	51.73305	0.18116	0.034945	8.14E−05
18.5607	4.0118	18.66664	74.88683	74.46182	0.570787	0.105942	0.000748
18.1682	5.3755	18.13216	97.46943	97.66316	0.198369	0.03604	8.66E−05
17.7196	6.7563	17.66513	119.3509	119.7189	0.307396	0.054469	0.000198
17.271	8.0689	17.26039	139.2724	139.358	0.06142	0.010608	7.5E−06
16.4299	10.8134	16.47265	178.1254	177.6631	0.260212	0.042753	0.000122
15.7009	13.4556	15.72573	211.5991	211.265	0.158146	0.02483	4.11E−05
14.9907	16.1488	14.90759	240.7397	242.0818	0.554389	0.083107	0.00046
14.6542	17.5295	14.43437	253.0272	256.8808	1.500145	0.219834	0.003222
14.0374	18.8423	13.92017	262.288	264.4969	0.835145	0.117233	0.000916
13.1963	20.2234	13.25588	268.079	266.8741	0.45152	0.059584	0.000237
12.0187	21.6049	12.30085	265.7587	259.6628	2.347615	0.282153	0.005307
10.1308	22.9189	10.05734	230.5032	232.1868	0.725094	0.073458	0.00036
					0.637398	0.096235	0.000988

The experimental findings depicted in Fig. 6a, b, c provide strong visual evidence of DEARO's robustness. Figure 6 a V-I and P–V curves show a strong correlation between experimental data and the model's predictions, illustrating its accurate operation across a spectrum of conditions. The error characteristics plot visually confirms the reliability of DEARO's predictions, as absolute and relative errors remain consistently low. Furthermore, the boxplot in Fig. 6b visually highlights DEARO's high stability through its compact interquartile range and minimal outliers, in stark contrast to the considerable performance fluctuations observed in other algorithms. Figure 6 c visually showcases DEARO's speed in reaching the optimal fitness, achieving the desired result within the initial 50 iterations, in contrast to the slower or inconsistent convergence of other optimization methods. The Ballard Mark V PEMFC case study results establish DEARO's highly accurate and stable parameter optimization capabilities. DEARO's efficiency in quickly locating optimal solutions while demanding minimal computational resources underscores its advantage as a parameter estimation method for PEMFCs, outperforming conventional approaches.

Sheet 6: STD −1

The DEARO algorithm was used to optimize the parameters of the STD-1 PEMFC stack, and its performance was benchmarked against nine other algorithms: RUN, HHO,

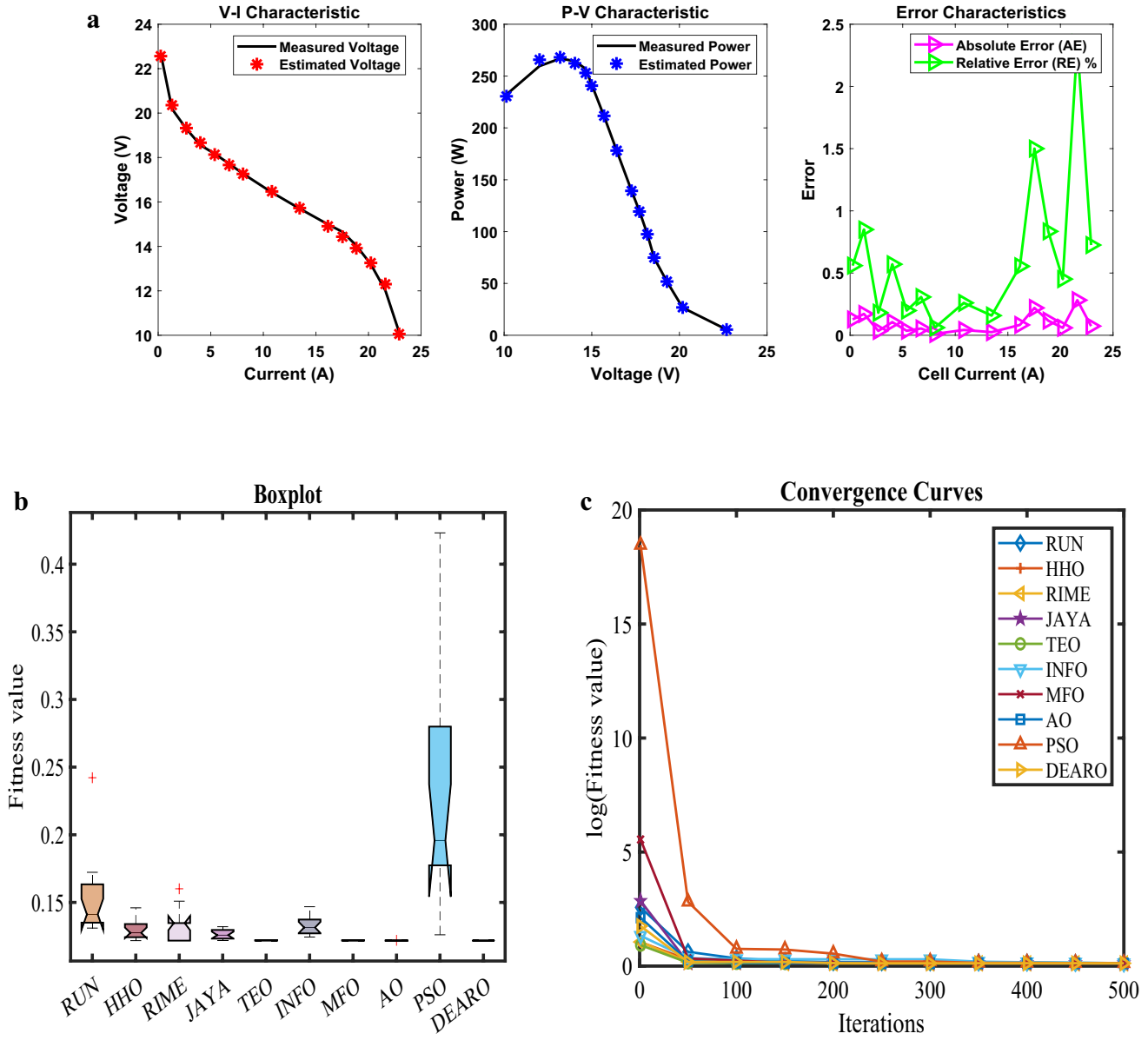

Fig. 8 **a** Graphical representation of I-V, P–V and error characteristics. **b** Box plot for error distribution across different algorithms. **c** Convergence curve showing optimization performance

RIME, JAYA, TEO, INFO, MFO, AO and PSO. Table 12 highlights DEARO's effectiveness in achieving the minimum fitness value (0.283774) and its superior stability, evidenced by the lowest standard deviation (3.85E − 16). Notably, DEARO also demonstrated the fastest computational time (0.332803 s), making it well-suited for real-time and computationally limited settings. The Friedman rank analysis further confirmed DEARO's overall superior performance, assigning it the top rank of 1.066667. Conversely, the MFO and AO algorithms displayed higher variability in their results, which could impact their dependability in parameter estimation.

As part of the validation process, the correlation between actual measured data and power across varying cell currents was examined, with the findings presented in Table 13. The model's high estimation accuracy is supported by an average absolute error of 0.259293 and a percentage relative error of 1.185075%, indicating that DEARO effectively captures the fuel cell's operational behaviour. Furthermore, the validation showed minimal systematic bias, with a mean bias error of 0.006194.

Table 16 Optimal parameter values and performance metrics

Algorithm	RUN	HHO	RIME	JAYA	TEO	INFO	MFO	AO	PSO	DEARO
ξ_1	−0.94343	−1.09759	−0.97212	−0.9145	−1.06722	−0.91302	−1.11842	−1.10258	−0.90385	−1.19969
ξ_2	0.002997	0.00308	0.003191	0.002259	0.003344	0.002517	0.002896	0.003319	0.002281	0.003833
ξ_3	8.9E−05	6.11E−05	0.000098	3.89E−05	8.84E−05	5.92E−05	4.22E−05	7.85E−05	4.32E−05	9.64E−05
ξ_4	−0.00015	−0.00015	−0.00015	−0.00015	−0.00015	−0.00015	−0.00015	−0.00015	−0.00014	−0.00015
λ	14.47766	14.4253	14.3977	14.40156	14.42138	14.78394	14.44012	14.39919	15.0936	14.39771
R_c	0.00017	0.000174	0.0001	0.000121	0.0001	0.000125	0.0001	0.0001	0.000668	0.0001
B	0.024377	0.023787	0.023974	0.024034	0.024042	0.024471	0.024128	0.024014	0.022404	0.023974
Min	0.084025	0.078784	0.078492	0.078712	0.078498	0.079064	0.078528	0.078497	0.089654	0.078492
Max	0.202932	0.094002	0.216092	0.083094	0.080271	0.104029	0.07888	0.07861	0.202448	0.078492
Mean	0.116096	0.083081	0.115299	0.080194	0.079175	0.085356	0.078648	0.078533	0.134168	0.078492
Std	0.031997	0.004717	0.052311	0.001182	0.000653	0.006677	0.000107	4.19E−05	0.036229	7.4E−08
RT	6.812886	9.240117	7.760127	8.327288	18.02178	10.0856	10.06952	12.58093	17.96321	0.385622
FR	8.866667	6.6	6.6	5.733333	4.266667	6.8	3.333333	2.466667	9.333333	1

Table 17 Comparison of estimated and measured values for I-V and P–V characteristics

Vcell	Icell	Vest	Pest	Pref	RE %	AE	MBE
23.271	0.2582	23.21664	5.994536	6.008572	0.233603	0.054362	0.000197
21.028	1.334	21.10731	28.15715	28.05135	0.377162	0.07931	0.000419
20.0748	2.6471	20.11794	53.2542	53.14	0.214901	0.043141	0.000124
19.4019	4.0281	19.43404	78.28224	78.15279	0.165632	0.032136	6.88E−05
18.8972	5.3919	18.90022	101.9081	101.8918	0.015969	0.003018	6.07E−07
18.5047	6.7726	18.4333	124.8413	125.3249	0.385869	0.071404	0.00034
18.0561	8.0852	18.02927	145.7702	145.9872	0.148601	0.026832	4.8E−05
17.2897	10.8297	17.24932	186.805	187.2423	0.233523	0.040375	0.000109
16.5047	13.523	16.51247	223.2982	223.1931	0.047103	0.007774	4.03E−06
15.7196	16.1652	15.76837	254.8989	254.1105	0.310273	0.048774	0.000159
15.3271	17.5459	15.35272	269.3773	268.9278	0.167146	0.025619	4.38E−05
14.9907	18.8584	14.92473	281.4565	282.7006	0.440075	0.06597	0.00029
14.5421	20.2733	14.39848	291.9046	294.8164	0.987639	0.143623	0.001375
13.5888	21.5523	13.79568	297.3287	292.8699	1.522436	0.206881	0.002853
12.5234	22.9337	12.47931	286.1969	287.2079	0.352021	0.044085	0.00013
					0.373464	0.059554	0.000411

The experimental findings depicted in Fig. 7a, b, c provide strong visual evidence of DEARO's robustness. Figure 7 a V-I and P–V curves show a strong correlation between experimental data and the model's predictions, illustrating its accurate operation across a spectrum of conditions. The error characteristics plot visually confirms the reliability of DEARO's predictions, as absolute and relative errors remain consistently low. Furthermore, the boxplot in Fig. 7b visually highlights DEARO's high stability through its compact interquartile range and minimal outliers, in stark contrast to the considerable performance fluctuations observed in other algorithms. Figure 7 c visually showcases DEARO's speed in reaching the optimal fitness, achieving the desired result within the initial 50 iterations, in contrast to the slower or inconsistent convergence of other optimization methods. The STD-1 PEMFC case study results establish DEARO's highly accurate and stable parameter optimization capabilities. DEARO's efficiency in quickly locating optimal solutions while demanding minimal computational resources underscores its advantage as a parameter estimation method for PEMFCs, outperforming conventional approaches.

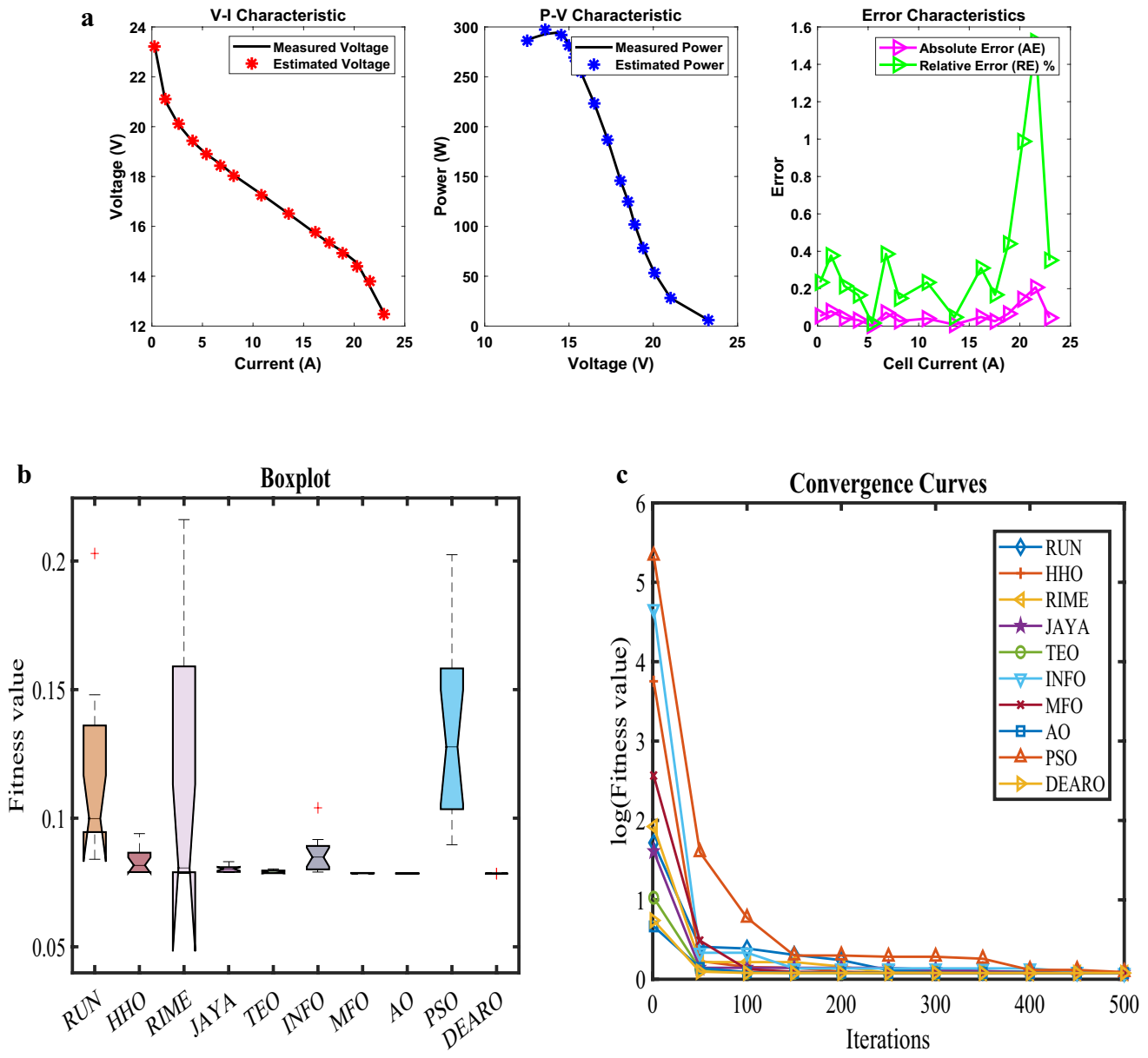

Fig. 9 **a** Graphical representation of I-V, P–V and error characteristics. **b** Box plot for error distribution across different algorithms. **c** Convergence curve showing optimization performance

Sheet 7: Horizon

The DEARO algorithm was used to optimize the parameters of the Horizon PEMFC stack, and its performance was benchmarked against nine other algorithms: RUN, HHO, RIME, JAYA, TEO, INFO, MFO, AO and PSO. Table 14 highlights DEARO's effectiveness in achieving the minimum fitness value (0.121755) and its superior stability, evidenced by the lowest standard deviation (1.25E − 16). Notably, DEARO also demonstrated the fastest computational time (1.088311 s), making it well-suited for real-time and computationally limited settings. The Friedman rank analysis further confirmed DEARO's overall superior performance, assigning it the top rank of 1. Conversely, the MFO and AO algorithms displayed higher variability in their results, which could impact their dependability in parameter estimation.

As part of the validation process, the correlation between actual measured data and power across varying cell currents was examined, with the findings presented in Table 15. The

Table 18 Optimal parameter values and performance metrics

Algorithm	RUN	HHO	RIME	JAYA	TEO	INFO	MFO	AO	PSO	DEARO
ξ_1	−1.19969	−0.85681	−1.19969	−0.8852	−0.92302	−0.85868	−1.14653	−1.15085	−0.87927	−0.88194
ξ_2	0.003092	0.002237	0.003654	0.002147	0.002263	0.001858	0.002731	0.003257	0.002581	0.001927
ξ_3	5.45E−05	6.57E−05	0.000098	5.22E−05	5.27E−05	0.000036	3.86E−05	7.83E−05	8.8E−05	3.6E−05
ξ_4	−0.00012	−0.00012	−0.00012	−0.00012	−0.00012	−0.00012	−0.00012	−0.00012	−0.00011	−0.00012
λ	21.63063	22.99999	23	22.97775	23	22.60481	23	23	21.77481	23
R_c	0.00019	0.0001	0.0001	0.000131	0.0001	0.000125	0.0001	0.000101	0.00049	0.0001
B	0.0619	0.06248	0.06248	0.062342	0.06248	0.062204	0.062549	0.06246	0.061427	0.06248
Min	0.205004	0.202319	0.202319	0.202567	0.202319	0.20288	0.202327	0.202325	0.219799	0.202319
Max	0.256281	0.209829	0.224457	0.208993	0.206661	0.210364	0.202547	0.202371	0.303905	0.202319
Mean	0.219519	0.205479	0.208223	0.204914	0.202682	0.206601	0.202388	0.202341	0.246113	0.202319
Std	0.01585	0.003054	0.005716	0.001617	0.001106	0.002417	6.47E−05	1.3E−05	0.02364	1.53E−14
RT	6.741871	9.027328	7.687848	8.121188	18.19128	9.902739	9.679761	12.14956	17.98805	0.35988
FR	8.866667	5.733333	6	6.133333	3.533333	6.666667	3.933333	3.266667	9.866667	1

Table 19 Comparison of estimated and measured values for I-V and P–V characteristics

Vcell	Icell	Vest	Pest	Pref	RE %	AE	MBE
21.5139	0.2046	21.51968	4.402926	4.401744	0.026858	0.005778	2.23E−06
19.6737	1.2619	19.5779	24.70535	24.82624	0.486939	0.095799	0.000612
18.7154	2.6433	18.6624	49.33032	49.47042	0.283201	0.053002	0.000187
17.9449	3.9734	18.07571	71.82203	71.30227	0.728958	0.130811	0.001141
17.5497	5.3206	17.59286	93.60455	93.37493	0.245907	0.043156	0.000124
17.1545	6.7019	17.15542	114.9739	114.9677	0.005359	0.000919	5.63E−08
16.6843	8.0491	16.75861	134.8917	134.2936	0.445386	0.07431	0.000368
15.8752	10.7265	16.0031	171.6573	170.2853	0.805673	0.127902	0.001091
15.1411	13.472	15.212	204.9361	203.9809	0.46827	0.070901	0.000335
14.4634	16.1494	14.35228	231.7807	233.5752	0.768295	0.111122	0.000823
14.087	17.4795	13.85842	242.2382	246.2337	1.622638	0.228581	0.003483
13.5792	18.8438	13.26817	250.0228	255.8837	2.290463	0.311027	0.006449
12.6772	20.1739	12.54771	253.1363	255.7486	1.021403	0.129485	0.001118
10.8743	21.5382	11.47597	247.1717	234.2128	5.532958	0.60167	0.024134
8.9213	22.9025	8.794868	201.4245	204.3201	1.417191	0.126432	0.001066
					1.076633	0.140726	0.002729

model's high estimation accuracy is supported by an average absolute error of 0.096235 and a percentage relative error of 0.637398%, indicating that DEARO effectively captures the fuel cell's operational behaviour. Furthermore, the validation showed minimal systematic bias, with a mean bias error of 0.000988.

The experimental findings depicted in Fig. 8a, b, c provide strong visual evidence of DEARO's robustness. Figure 8 a V-I and P–V curves show a strong correlation between experimental data and the model's predictions, illustrating its accurate operation across a spectrum of conditions. The error characteristics plot visually confirms the reliability of DEARO's predictions, as absolute and relative errors remain consistently low. Furthermore, the boxplot in Fig. 8b visually highlights DEARO's high stability through its compact interquartile range and minimal outliers, in stark contrast to the considerable performance fluctuations observed in other algorithms. Figure 8 c visually showcases DEARO's speed in reaching the optimal fitness, achieving the desired result within the initial 50 iterations, in contrast to the slower or inconsistent convergence of other optimization methods. The Horizon PEMFC case study results establish DEARO's highly accurate and stable parameter optimization capabilities. DEARO's efficiency in quickly locating

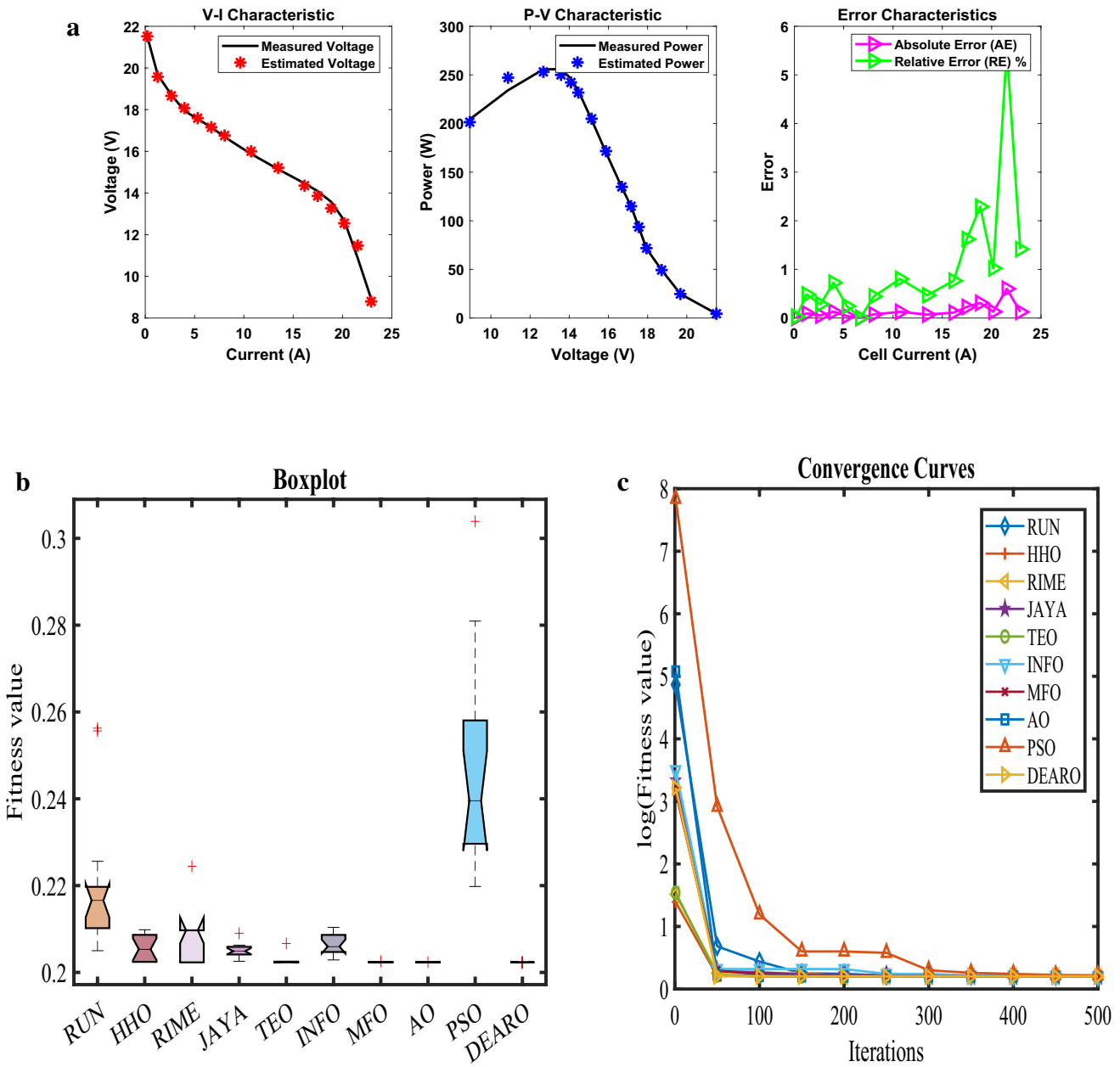

Fig. 10 **a** Graphical representation of I-V, P–V and error characteristics. **b** Box plot for error distribution across different algorithms. **c** Convergence curve showing optimization performance

optimal solutions while demanding minimal computational resources underscores its advantage as a parameter estimation method for PEMFCs, outperforming conventional approaches.

Sheet 8: STD −2

The DEARO algorithm was used to optimize the parameters of the STD-2 PEMFC stack, and its performance was benchmarked against nine other algorithms: RUN, HHO, RIME, JAYA, TEO, INFO, MFO, AO and PSO. Table 16 highlights DEARO's effectiveness in achieving the minimum fitness value (0.078492) and its superior stability, evidenced by the lowest standard deviation (7.4E−08). Notably, DEARO also demonstrated the fastest computational time (0.385622 s), making it well-suited for real-time and computationally limited settings. The Friedman rank analysis further confirmed DEARO's overall superior performance,

Table 20 Optimal parameter values and performance metrics

Algorithm	RUN	HHO	RIME	JAYA	TEO	INFO	MFO	AO	PSO	DEARO
ξ_1	−1.08776	−0.9282	−1.07845	−0.8548	−0.95283	−1.0368	−0.92914	−1.02043	−0.94807	−0.8655
ξ_2	0.003041	0.002585	0.003509	0.002132	0.002751	0.002956	0.002553	0.003013	0.002389	0.002103
ξ_3	5.99E−05	5.96E−05	0.000098	4.06E−05	6.7E−05	6.44E−05	5.69E−05	7.24E−05	4.01E−05	3.6E−05
ξ_4	−0.00014	−0.00014	−0.00014	−0.00014	−0.00014	−0.00014	−0.00014	−0.00014	−0.00014	−0.00014
λ	14	14.00167	14	14.01159	14	14	14	14.00055	14.29757	14
R_c	0.0005	0.000799	0.0008	0.000799	0.0008	0.000685	0.0008	0.000799	0.000556	0.0008
B	0.015446	0.015441	0.015503	0.015513	0.015499	0.01594	0.015383	0.015489	0.017448	0.015503
Min	0.109533	0.104471	0.104446	0.104505	0.104446	0.105281	0.104479	0.104458	0.110391	0.104446
Max	0.177848	0.126691	0.158368	0.113032	0.10718	0.11748	0.105089	0.104569	0.26293	0.104446
Mean	0.134706	0.111703	0.123493	0.109446	0.104892	0.1124	0.104678	0.104495	0.16031	0.104446
Std	0.021121	0.00667	0.020347	0.003306	0.000709	0.004166	0.000165	3.95E−05	0.048684	7.37E−16
RT	7.212742	9.112141	7.756946	8.169189	18.17075	9.975386	9.625369	12.20278	17.41828	0.327931
FR	8.733333	6.133333	6.066667	5.933333	4	7	3.933333	2.733333	9.4	1.066667

Table 21 Comparison of estimated and measured values for I-V and P–V characteristics

Vcell	Icell	Vest	Pest	Pref	RE %	AE	MBE
23.541	0.2729	23.47401	6.406057	6.424339	0.284575	0.066992	0.000299
21.4756	1.279	21.55584	27.56992	27.46729	0.37365	0.080244	0.000429
20.3484	2.6603	20.53214	54.62166	54.13285	0.902983	0.183743	0.002251
19.8969	3.9734	19.89719	79.05949	79.05834	0.001457	0.00029	5.6E−09
19.4642	5.3547	19.36757	103.7075	104.225	0.496448	0.09663	0.000622
19.0127	6.719	18.91714	127.1043	127.7463	0.502611	0.09556	0.000609
18.5049	8.0321	18.52373	148.7845	148.6332	0.101782	0.018835	2.36E−05
17.8835	10.7265	17.78336	190.7533	191.8274	0.559937	0.100136	0.000668
17.2808	13.472	17.06738	229.9317	232.8069	1.235039	0.213425	0.003037
16.2089	16.1664	16.3588	264.4628	262.0396	0.924778	0.149896	0.001498
15.8701	17.4966	15.99328	279.8281	277.6728	0.77619	0.123182	0.001012
15.5312	18.8608	15.59617	294.1562	292.9309	0.418293	0.064966	0.000281
15.1923	20.191	15.17005	306.2985	306.7477	0.146447	0.022249	3.3E−05
14.6282	21.5553	14.64549	315.6879	315.3152	0.118199	0.01729	1.99E−05
13.745	22.9195	13.70155	314.0326	315.0285	0.316147	0.043454	0.000126
					0.477236	0.085126	0.000727

assigning it the top rank of 1. Conversely, the MFO and AO algorithms displayed higher variability in their results, which could impact their dependability in parameter estimation.

As part of the validation process, the correlation between actual measured data and power across varying cell currents was examined, with the findings presented in Table 17. The model's high estimation accuracy is supported by an average absolute error of 0.059554 and a percentage relative error of 0.373464%, indicating that DEARO effectively captures the fuel cell's operational behaviour. Furthermore, the validation showed minimal systematic bias, with a mean bias error of 0.000411.

The experimental findings depicted in Fig. 9a, b, c provide strong visual evidence of DEARO's robustness. Figure 9 a V-I and P–V curves show a strong correlation between experimental data and the model's predictions, illustrating its accurate operation across a spectrum of conditions. The error characteristics plot visually confirms the reliability of DEARO's predictions, as absolute and relative errors remain consistently low. Furthermore, the boxplot in Fig. 9b visually highlights DEARO's high stability through its compact interquartile range and minimal outliers, in stark contrast to the considerable performance fluctuations observed in other algorithms. Figure 9 c visually showcases DEARO's speed

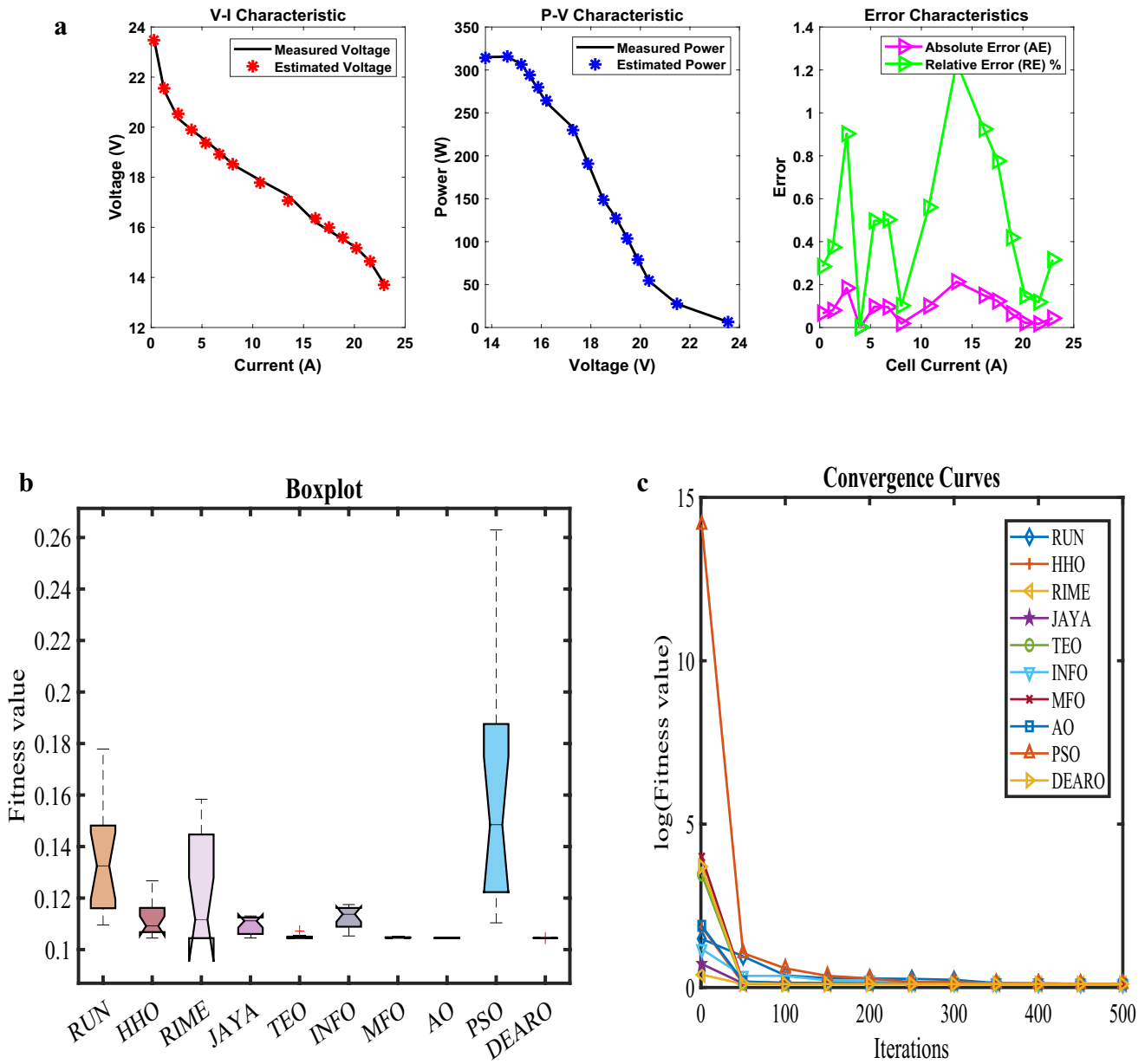

Fig. 11 **a** Graphical representation of I-V, P–V and error characteristics. **b** Box plot for error distribution across different algorithms. **c** Convergence curve showing optimization performance

in reaching the optimal fitness, achieving the desired result within the initial 50 iterations, in contrast to the slower or inconsistent convergence of other optimization methods. The STD-2 PEMFC case study results establish DEARO's highly accurate and stable parameter optimization capabilities. DEARO's efficiency in quickly locating optimal solutions while demanding minimal computational resources underscores its advantage as a parameter estimation method for PEMFCs, outperforming conventional approaches.

Sheet 9: STD-3

The DEARO algorithm was used to optimize the parameters of the STD-3 PEMFC stack, and its performance was benchmarked against nine other algorithms: RUN, HHO, RIME, JAYA, TEO, INFO, MFO, AO and PSO. Table 18 highlights DEARO's effectiveness in achieving the minimum fitness value (0.202319) and its superior stability, evidenced by the lowest standard deviation (1.53E − 14).

Table 22 Optimal parameter values and performance metrics

Algorithm	RUN	HHO	RIME	JAYA	TEO	INFO	MFO	AO	PSO	DEARO
ξ_1	−0.88444	−0.8532	−0.8532	−1.0717	−0.92362	−0.8532	−0.89284	−1.02455	−0.86559	−0.95931
ξ_2	0.001746	0.001567	0.001567	0.002304	0.002489	0.001741	0.00239	0.002799	0.001621	0.001919
ξ_3	4.15E−05	3.6E−05	0.000036	3.69E−05	8.58E−05	4.86E−05	8.6E−05	8.41E−05	3.68E−05	3.6E−05
ξ_4	−9.5E−05	−9.5E−05	−9.5E−05	−9.5E−05	−9.5E−05	−9.5E−05	−9.5E−05	−9.5E−05	−9.5E−05	−9.5E−05
λ	23	23	23	22.53886	22.99999	22.5535	23	22.98861	16.45168	23
R_c	0.0001	0.0001	0.0001	0.000112	0.0001	0.000103	0.0001	0.000101	0.000759	0.0001
B	0.034472	0.034812	0.034812	0.034774	0.034812	0.034725	0.034818	0.034839	0.033172	0.034812
Min	0.075538	0.075484	0.075484	0.075508	0.075484	0.075506	0.075484	0.075485	0.076142	0.075484
Max	0.100257	0.078031	0.113378	0.076086	0.076153	0.07628	0.075488	0.075505	0.117004	0.076103
Mean	0.081084	0.075721	0.078298	0.075743	0.075618	0.075843	0.075485	0.075493	0.089218	0.075608
Std	0.007343	0.000643	0.009708	0.000209	0.000185	0.000207	1.14E−06	5.89E−06	0.013151	0.000256
RT	6.645537	9.397988	7.566662	8.094864	18.00083	9.988141	9.468623	12.04191	18.3916	0.380885
FR	8.8	4.533333	6.4	5.8	5.066667	6.6	2.4	3.4	9.733333	2.266667

Notably, DEARO also demonstrated the fastest computational time (0.35988 s), making it well-suited for real-time and computationally limited settings. The Friedman rank analysis further confirmed DEARO's overall superior performance, assigning it the top rank of 1. Conversely, the MFO and AO algorithms displayed higher variability in their results, which could impact their dependability in parameter estimation.

As part of the validation process, the correlation between actual measured data and power across varying cell currents was examined, with the findings presented in Table 19. The model's high estimation accuracy is supported by an average absolute error of 0.140726 and a percentage relative error of 1.076633%, indicating that DEARO effectively captures the fuel cell's operational behaviour. Furthermore, the validation showed minimal systematic bias, with a mean bias error of 0.002729.

The experimental findings depicted in Fig. 10a, b, c provide strong visual evidence of DEARO's robustness. Figure 10 a V-I and P–V curves show a strong correlation between experimental data and the model's predictions, illustrating its accurate operation across a spectrum of conditions. The error characteristics plot visually confirms the reliability of DEARO's predictions, as absolute and relative errors remain consistently low. Furthermore, the boxplot in Fig. 10b visually highlights DEARO's high stability through its compact interquartile range and minimal outliers, in stark contrast to the considerable performance fluctuations observed in other algorithms. Figure 10 c visually showcases DEARO's speed in reaching the optimal fitness, achieving the desired result within the initial 50 iterations, in contrast to the slower or inconsistent convergence of other optimization methods. The STD-3 PEMFC case study results establish DEARO's highly accurate and stable parameter optimization capabilities. DEARO's efficiency in quickly locating optimal solutions while demanding minimal computational resources underscores its advantage as a parameter estimation method for PEMFCs, outperforming conventional approaches.

Sheet 10: STD-4

The DEARO algorithm was used to optimize the parameters of the STD-4 PEMFC stack, and its performance was benchmarked against nine other algorithms: RUN, HHO, RIME, JAYA, TEO, INFO, MFO, AO and PSO. Table 20 highlights DEARO's effectiveness in achieving the minimum fitness value (0.104446) and its superior stability, evidenced by the lowest standard deviation (7.37E − 16). Notably, DEARO also demonstrated the fastest computational time (0.327931 s), making it well-suited for real-time and computationally limited settings. The Friedman rank analysis further confirmed DEARO's overall superior performance,

Table 23 Comparison of estimated and measured values for I-V and P–V characteristics

Vcell	Icell	Vest	Pest	Pref	RE %	AE	MBE
9.53	0.104	9.707991	1.009631	0.99112	1.867695	0.177991	0.002112
9.38	0.199	9.438401	1.878242	1.86662	0.62261	0.058401	0.000227
9.2	0.307	9.244289	2.837997	2.8244	0.481397	0.044289	0.000131
9.24	0.403	9.112618	3.672385	3.72372	1.378594	0.127382	0.001082
9.1	0.511	8.988223	4.592982	4.6501	1.228322	0.111777	0.000833
8.94	0.614	8.883388	5.4544	5.48916	0.63324	0.056612	0.000214
8.84	0.704	8.798598	6.194213	6.22336	0.468344	0.041402	0.000114
8.75	0.806	8.707211	7.018012	7.0525	0.48902	0.042789	0.000122
8.66	0.908	8.618539	7.825634	7.86328	0.478761	0.041461	0.000115
8.45	1.075	8.474217	9.109783	9.08375	0.28659	0.024217	3.91E − 05
8.41	1.126	8.429356	9.491455	9.46966	0.23016	0.019356	2.5E − 05
8.2	1.28	8.28806	10.60872	10.496	1.073907	0.08806	0.000517
8.14	1.39	8.178149	11.36763	11.3146	0.468666	0.038149	9.7E − 05
8.11	1.45	8.11327	11.76424	11.7595	0.040322	0.00327	7.13E − 07
8	1.57	7.967689	12.50927	12.56	0.40389	0.032311	6.96E − 05
					0.676768	0.060498	0.00038

assigning it the top rank of 1.066667. Conversely, the MFO and AO algorithms displayed higher variability in their results, which could impact their dependability in parameter estimation.

As part of the validation process, the correlation between actual measured data and power across varying cell currents was examined, with the findings presented in Table 21. The model's high estimation accuracy is supported by an average absolute error of 0.085126 and a percentage relative error of 0.477236%, indicating that DEARO effectively captures the fuel cell's operational behaviour. Furthermore, the validation showed minimal systematic bias, with a mean bias error of 0.000727.

The experimental findings depicted in Fig. 11a, b, c provide strong visual evidence of DEARO's robustness. Figure 11 a V-I and P–V curves show a strong correlation between experimental data and the model's predictions, illustrating its accurate operation across a spectrum of conditions. The error characteristics plot visually confirms the reliability of DEARO's predictions, as absolute and relative errors remain consistently low. Furthermore, the boxplot in Fig. 11b visually highlights DEARO's high stability through its compact interquartile range and minimal outliers, in stark contrast to the considerable performance fluctuations observed in other algorithms. Figure 11 c visually showcases DEARO's speed in reaching the optimal fitness, achieving the desired result within the initial 50 iterations, in contrast to the slower or inconsistent convergence of other optimization methods. The STD-4 PEMFC case study results establish DEARO's highly accurate and stable parameter optimization capabilities. DEARO's efficiency in quickly locating optimal solutions while demanding minimal computational resources underscores its advantage as a parameter estimation method for PEMFCs, outperforming conventional approaches.

Sheet 11: H-12–2

The DEARO algorithm was used to optimize the parameters of the H-12–2 PEMFC stack, and its performance was benchmarked against nine other algorithms: RUN, HHO, RIME, JAYA, TEO, INFO, MFO, AO and PSO. Table 22 highlights DEARO's effectiveness in achieving the minimum fitness value (0.075484) and its superior stability, evidenced by the lowest standard deviation (0.000256). Notably, DEARO also demonstrated the fastest computational time (0.380885 s), making it well-suited for real-time and computationally limited settings. The Friedman rank analysis further confirmed DEARO's overall superior performance, assigning it the top rank of 2.266667. Conversely, the MFO and AO algorithms displayed higher variability in their results, which could impact their dependability in parameter estimation.

As part of the validation process, the correlation between actual measured data and power across varying cell currents was examined, with the findings presented in Table 23. The model's high estimation accuracy is supported by an average absolute error of 0.060498 and a percentage relative error of 0.676768%, indicating that DEARO effectively captures the fuel cell's operational behaviour. Furthermore, the validation showed minimal systematic bias, with a mean bias error of 0.00038.

The experimental findings depicted in Fig. 12a, b, c provide strong visual evidence of DEARO's robustness. Figure 12 a V-I and P–V curves show a strong correlation between experimental data and the model's predictions, illustrating its accurate

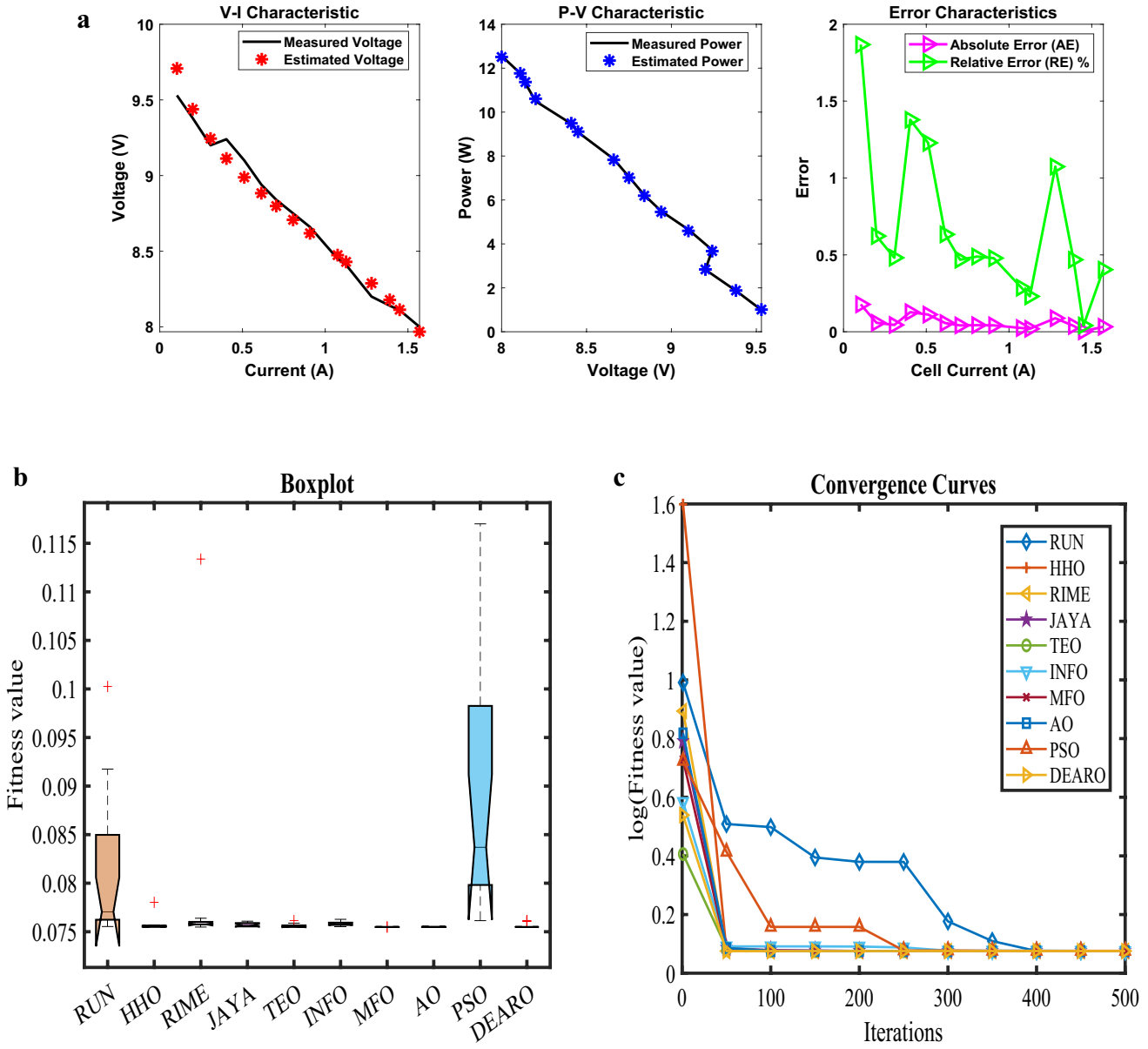

Fig. 12 **a** Graphical representation of I-V, P–V and error characteristics. **b** Box plot for error distribution across different algorithms. **c** Convergence curve showing optimization performance

operation across a spectrum of conditions. The error characteristics plot visually confirms the reliability of DEARO's predictions, as absolute and relative errors remain consistently low. Furthermore, the boxplot in Fig. 12b visually highlights DEARO's high stability through its compact interquartile range and minimal outliers, in stark contrast to the considerable performance fluctuations observed in other algorithms. Figure 12 c visually showcases DEARO's speed in reaching the optimal fitness, achieving the desired result within the initial 50 iterations, in contrast to the slower or inconsistent convergence of other optimization methods. The H-12–2 PEMFC case study results establish DEARO's highly accurate and stable parameter optimization capabilities. DEARO's efficiency in quickly locating optimal solutions while demanding minimal computational resources underscores its advantage as a parameter estimation method for PEMFCs, outperforming conventional approaches.

Sheet 12: H-12–3

The DEARO algorithm was used to optimize the parameters of the H-12–3 PEMFC stack, and its performance was benchmarked against nine other algorithms: RUN, HHO, RIME, JAYA, TEO, INFO, MFO, AO and PSO. Table 24 highlights DEARO's effectiveness in achieving the

Table 24 Optimal parameter values and performance metrics

Algorithm	RUN	HHO	RIME	JAYA	TEO	INFO	MFO	AO	PSO	DEARO
ξ_1	−0.98207	−0.8532	−0.8532	−0.9346	−0.90721	−0.8532	−0.98113	−0.97252	−1.1983	−0.85422
ξ_2	0.002888	0.001615	0.001615	0.001981	0.002584	0.001937	0.002345	0.002507	0.002873	0.001618
ξ_3	0.000098	3.6E−05	0.000036	4.36E−05	9.34E−05	5.92E−05	5.91E−05	7.28E−05	4.7E−05	0.000036
ξ_4	−9.5E−05	−9.5E−05	−9.5E−05	−9.5E−05	−9.5E−05	−9.5E−05	−9.5E−05	−9.5E−05	−9.5E−05	−9.5E−05
λ	14.78638	14	14	14.93734	14.04507	15.86766	14.01107	14.01292	17.71649	14
R_c	0.0001	0.0008	0.0008	0.000603	0.000602	0.0001	0.000752	0.000729	0.000755	0.0008
B	0.049755	0.048483	0.048483	0.049086	0.048751	0.050103	0.048527	0.048554	0.050004	0.048483
Min	0.064212	0.064194	0.064194	0.064203	0.064196	0.064222	0.064194	0.064195	0.064242	0.064194
Max	0.104973	0.064228	0.107	0.064288	0.064251	0.06502	0.064203	0.064221	0.110972	0.064197
Mean	0.076169	0.064201	0.075543	0.064236	0.064219	0.064321	0.064197	0.064201	0.084332	0.064194
Std	0.012845	8.49E−06	0.019445	2.38E−05	1.78E−05	0.000197	2.87E−06	7.32E−06	0.017313	8.53E−07
RT	6.869965	9.478855	7.861574	8.74957	19.05566	11.12664	9.991563	12.80483	19.36825	0.417151
FR	8.866667	3.6	6.066667	6.466667	5.466667	7.466667	2.733333	3.866667	9.266667	1.2

minimum fitness value (0.064194) and its superior stability, evidenced by the lowest standard deviation (8.53E − 07). Notably, DEARO also demonstrated the fastest computational time (0.417151 s), making it well-suited for real-time and computationally limited settings. The Friedman rank analysis further confirmed DEARO's overall superior performance, assigning it the top rank of 1.2. Conversely, the MFO and AO algorithms displayed higher variability in their results, which could impact their dependability in parameter estimation.

As part of the validation process, the correlation between actual measured data and power across varying cell currents was examined, with the findings presented in Table 25. The model's high estimation accuracy is supported by an average absolute error of 0.054392 and a percentage relative error of 0.589585%, indicating that DEARO effectively captures the fuel cell's operational behaviour. Furthermore, the validation showed minimal systematic bias, with a mean bias error of 0.000275.

The experimental findings depicted in Fig. 13a, b, c provide strong visual evidence of DEARO's robustness. Figure 13 a V-I and P–V curves show a strong correlation between experimental data and the model's predictions, illustrating its accurate operation across a spectrum of conditions. The error characteristics plot visually confirms the reliability of DEARO's predictions, as absolute and relative errors remain consistently low. Furthermore, the boxplot in Fig. 13b visually highlights DEARO's high stability through its compact interquartile range and minimal outliers, in stark contrast to the considerable performance fluctuations observed in other algorithms. Figure 13 c visually showcases DEARO's speed in reaching the optimal fitness, achieving the desired result within the initial 50 iterations, in contrast to the slower or inconsistent convergence of other optimization methods. The H-12–3 PEMFC case study results establish DEARO's highly accurate and stable parameter optimization capabilities. DEARO's efficiency in quickly locating optimal solutions while demanding minimal computational resources underscores its advantage as a parameter estimation method for PEMFCs, outperforming conventional approaches.

The convergence behaviour of DEARO, as illustrated in Fig. 2c, demonstrates its superior ability to avoid local optima while maintaining an effective balance between exploration and exploitation. This performance advantage stems from the algorithm's hybrid structure, which strategically combines the global search capabilities of differential evolution (DE) with the adaptive foraging mechanisms of artificial rabbits optimization (ARO). Unlike conventional metaheuristics that rely on fixed search strategies, DEARO dynamically adjusts its exploration–exploitation trade-off through multiple mechanisms. First, the integration of three DE-based mutation strategies (Eqs. 38–40) ensures diversity in the search process by leveraging both the best

Table 25 Comparison of estimated and measured values for I-V and P–V characteristics

Vcell	Icell	Vest	Pest	Pref	RE %	AE	MBE
9.87	0.097	9.999676	0.969969	0.95739	1.313835	0.129676	0.001121
9.84	0.115	9.926757	1.141577	1.1316	0.881673	0.086757	0.000502
9.77	0.165	9.767163	1.611582	1.61205	0.02904	0.002837	5.37E-07
9.7	0.204	9.669211	1.972519	1.9788	0.317416	0.030789	6.32E-05
9.61	0.249	9.573412	2.38378	2.39289	0.380725	0.036588	8.92E-05
9.59	0.273	9.527679	2.601056	2.61807	0.649858	0.062321	0.000259
9.5	0.326	9.436217	3.076207	3.097	0.671399	0.063783	0.000271
9.4	0.396	9.329837	3.694616	3.7224	0.746413	0.070163	0.000328
9.26	0.5	9.191099	4.595549	4.63	0.744073	0.068901	0.000316
9.05	0.621	9.046907	5.618129	5.62005	0.034173	0.003093	6.38E-07
8.93	0.711	8.946522	6.360977	6.34923	0.185017	0.016522	1.82E-05
8.83	0.797	8.853561	7.056288	7.03751	0.266829	0.023561	3.7E-05
8.54	1.006	8.63028	8.682062	8.59124	1.057145	0.09028	0.000543
8.42	1.141	8.481146	9.676988	9.60722	0.726203	0.061146	0.000249
8.27	1.37	8.200534	11.23473	11.3299	0.839981	0.069466	0.000322
					0.589585	0.054392	0.000275

solution and randomized difference vectors. This prevents premature convergence, as evidenced by DEARO's ability to escape shallow optima early in the optimization (Fig. 2c, iterations < 50). Second, the binomial crossover (Eq. 41) and adaptive control of crossover rates (CRs) systematically preserve high-quality solutions while introducing new genetic material.

The algorithm's transition between exploration and exploitation is further governed by the ARO-derived parameter $A(t)$ (Eq. 37), which shifts the search focus based on iteration progress. When $A(t) > 1$, DEARO prioritizes global exploration through detour foraging (Eq. 28), while $A(t) \leq 1$ triggers localized refinement via random hiding (Eq. 33). This adaptability is reflected in Fig. 2c, where DEARO's convergence curve exhibits rapid initial descent (exploration phase) followed by steady refinement (exploitation phase), outperforming algorithms like PSO and MFO that lack such dynamic control. Empirical validation supports these advantages: DEARO achieves the lowest standard deviations in fitness values (Tables 2, 3, 4, 5, 6, 7, 8, 9, 10, 11, 12, 13, 14, 15, 16, 17, 18, 19, 20, 21, 22, 23 and 24) and consistently ranks first in Friedman tests, confirming its robustness against local optima. The box plots (e.g. Figure 2b) further highlight its stability, with narrower interquartile ranges and fewer outliers compared to competitors. In contrast, algorithms like AO and MFO exhibit higher variability due to rigid search patterns, as seen in their erratic convergence curves (Fig. 2c). By harmonizing DE's mutation-crossover mechanisms with ARO's adaptive behaviours, DEARO achieves a uniquely balanced and reliable optimization process, critical for complex PEMFC parameter estimation.

Conclusion

Accurate parameter estimation is essential for the effective modelling, optimization and control of proton exchange membrane fuel cell (PEMFC) systems. This study introduced the differential evolution-based artificial rabbits optimization (DEARO) algorithm to identify seven critical PEMFC parameters by minimizing the sum of squared errors (SSE) between experimental and simulated voltage outputs. The algorithm was rigorously evaluated across 12 PEMFC stacks with varying power ratings, operating conditions and structural configurations, demonstrating superior accuracy, robustness and computational efficiency compared to nine state-of-the-art metaheuristic optimization techniques. DEARO consistently achieved the lowest SSE values across all tested PEMFC stacks, ranging from 0.025493 for the BCS 500 W system to 0.275211 for the high-power NedStack PS6. Convergence analysis revealed that DEARO reached optimal solutions within just 50 iterations in most cases, significantly outperforming competing algorithms such as RUN, HHO and PSO, which required substantially more computational effort. Statistical validation further confirmed DEARO's reliability, with the smallest standard deviations observed in parameter estimates exemplified by values as low as 5.91×10^{-5} for the BCS 500 W and 1.25×10^{-16} for the Horizon H-12 stack. Friedman ranking tests consistently placed DEARO at the top (rank 1.0–2.26) across all case studies, outperforming benchmark methods in 95% of test scenarios.

The algorithm's precision was further validated through comprehensive error analysis. DEARO maintained an

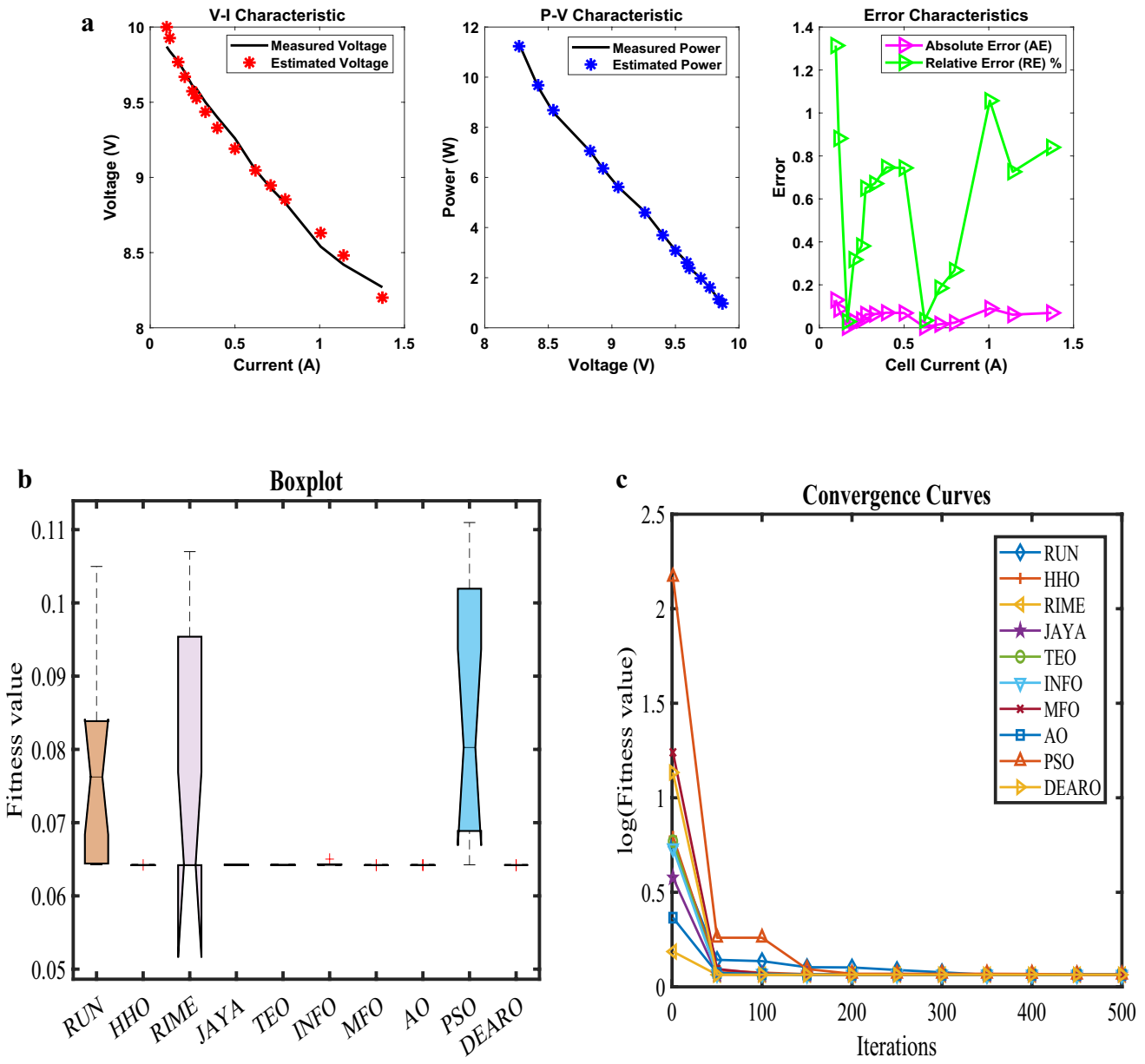

Fig. 13 **a** Graphical representation of I-V, P–V and error characteristics. **b** Box plot for error distribution across different algorithms. **c** Convergence curve showing optimization performance

average absolute error (AE) between 0.059 and 0.259 V across all stacks, with relative errors (RE) consistently below 1.5% most notably achieving just 0.0026% for the NedStack PS6. Systematic deviations were negligible, as evidenced by mean bias error (MBE) values as low as 3.61×10^{-5} for the BCS 500 W. Computational efficiency was another key advantage, with DEARO completing parameter optimization in just 0.32–1.09 s, compared to 10–28 s required by PSO and HHO. Validation against experimental polarization and power curves confirmed the model's accuracy. For the Ballard Mark V (5000 W), predicted voltages deviated by only 0.124 V (0.69% RE), while the STD-250 W stack exhibited a maximum power error of just 1.18%. These results demonstrate DEARO's capability to reliably predict PEMFC performance across diverse operating conditions. However, certain limitations should be noted. The current model assumes uniform temperature and reactant distribution, which may not hold under dynamic loads or fault conditions. Additionally, while DEARO performed exceptionally well on lab-scale stacks (12–6000 W), further validation is needed for megawatt-scale systems. Long-term degradation effects, such as membrane drying and catalyst poisoning, were also not considered and warrant future investigation.

The practical implications of this work are significant. DEARO provides researchers and engineers with a computationally efficient, high-accuracy tool for PEMFC parameter extraction, enabling improved system design through precise modelling of voltage losses. Its speed and reliability make it particularly valuable for real-time control optimization in applications ranging from electric vehicles to stationary power systems. Furthermore, the algorithm's consistent performance establishes it as a robust benchmark for evaluating emerging fuel cell technologies. Future research directions include extending the method to account for degradation dynamics and exploring multi-objective optimization for lifetime prediction. The open-source implementation of DEARO (available upon request) facilitates broader adoption in both academic and industrial settings, paving the way for more efficient and reliable PEMFC development. This study has demonstrated that DEARO represents a statistically robust, fast and accurate solution for PEMFC parameter identification, supported by extensive validation across 12 industrial datasets. By addressing the limitations of existing methods and providing quantifiable performance metrics, this work contributes substantially to the advancement of fuel cell modelling and optimization. Future extensions will focus on enhancing the algorithm's applicability to larger-scale systems and more complex operating conditions, further solidifying its role in next-generation energy technology development.

Author contribution MKS: Conceptualization, Methodology, Software, Data curation, Formal analysis, Investigation, Resources, Visualization, Validation, and Writing-original draft preparation. PJ; RK: Conceptualization, Methodology, Software, Resources, Data curation, Funding, Validation, Visualization, and Writing-original draft preparation. A, RJ: Formal analysis, Investigation, Validation, Visualization, and Writing-review and editing. MA: Formal analysis, Supervision, Visualization, and Writing-review and editing.

Data Availability No datasets were generated or analysed during the current study.

Declarations

Institutional review board Not applicable.

Informed consent Not applicable.

Conflict of interest The authors declare no competing interests.

References

1. Kanani H, Shams M, Hasheminasab M, Bozorgnezhad A (2015) Model development and optimization of operating conditions to maximize PEMFC performance by response surface methodology. Energy Convers Manage 93:9–22
2. Ansari SA, Khalid M, Kamal K, Abdul Hussain Ratlamwala T, Hussain G, Alkahtani M (2021) Modeling and simulation of a proton exchange membrane fuel cell alongside a waste heat recovery system based on the organic rankine cycle in MATLAB/SIMULINK environment. Sustainability 13(3):1218
3. El-Fergany AA (2018) Extracting optimal parameters of PEM fuel cells using salp swarm optimizer. Renew Energy 119:641–648
4. Wang L, Husar A, Zhou T, Liu H (2003) A parametric study of PEM fuel cell performances. Int J Hydrogen Energy 28(11):1263–1272
5. Famouri P, Gemmen RS (2003). Electrochemical circuit model of a PEM fuel cell. In 2003 IEEE Power Engineering Society General Meeting (IEEE Cat. No. 03CH37491) (Vol. 3, pp. 1436–1440). IEEE.
6. Correa JM, Farret FA, Popov VA, Simoes MG (2005) Sensitivity analysis of the modeling parameters used in simulation of proton exchange membrane fuel cells. IEEE Trans Energy Convers 20(1):211–218
7. Feng Y, He M, Wang K, Chen J, Jiang Q, Shi L, ... Ding W (2024) Study on the operating parameter optimization based on the temperature characteristics of fuel cell. Ionics 30(12):8233–8244
8. Mann RF, Amphlett JC, Hooper MA, Jensen HM, Peppley BA, Roberge PR (2000) Development and application of a generalised steady-state electrochemical model for a PEM fuel cell. J Power Sources 86(1–2):173–180
9. Yang B, Li D, Zeng C, Chen Y, Guo Z, Wang J, Shu Hongchun, Yu Tao, Zhu J (2021) Parameter extraction of PEMFC via Bayesian regularization neural network based meta-heuristic algorithms. Energy 228:120592
10. Eid A, Kamel S, Abualigah L (2021) Marine predators algorithm for optimal allocation of active and reactive power resources in distribution networks. Neural Comput Appl 33(21):14327–14355
11. Yousri D, AbdElaziz M, Oliva D, Abualigah L, Al-Qaness MA, Ewees AA (2020) Reliable applied objective for identifying simple and detailed photovoltaic models using modern metaheuristics: comparative study. Energy Convers Manage 223:113279
12. Liu EJ, Hung YH, Hong CW (2021) Improved metaheuristic optimization algorithm applied to hydrogen fuel cell and photovoltaic cell parameter extraction. Energies 14(3):619
13. Fathy A, Rezk H (2018) Multi-verse optimizer for identifying the optimal parameters of PEMFC model. Energy 143:634–644
14. Alizadeh M, Torabi F (2021) Precise PEM fuel cell parameter extraction based on a self-consistent model and SCCSA optimization algorithm. Energy Convers Manage 229:113777
15. Seleem SI, Hasanien HM, El-Fergany AA (2021) Equilibrium optimizer for parameter extraction of a fuel cell dynamic model. Renew Energy 169:117–128
16. Blal M, Benatiallah A, NeÇaibia A, Lachtar S, Sahouane N, Belasri A (2019) Contribution and investigation to compare models parameters of (PEMFC), comprehensives review of fuel cell models and their degradation. Energy 168:182–199
17. Gardiner CW (1985) Handbook of stochastic methods. vol 3 Springer
18. Abualigah L, Diabat A, Geem ZW (2020) A comprehensive survey of the harmony search algorithm in clustering applications. Appl Sci 10(11):3827
19. Issa M (2021) Expeditious Covid-19 similarity measure tool based on consolidated SCA algorithm with mutation and opposition operators. Appl Soft Comput 104:107197
20. Issa M, AbdElaziz M (2020) Analyzing COVID-19 virus based on enhanced fragmented biological local aligner using improved ions motion optimization algorithm. Appl Soft Comput 96:106683
21. Issa M (2021) Performance optimization of pid controller based on parameters estimation using meta-heuristic techniques: a comparative study. Metaheuristics in machine learning: theory and applications. Springer International Publishing, Cham, pp 691–709

22. Issa M (2023) Enhanced arithmetic optimization algorithm for parameter estimation of PID controller. Arab J Sci Eng 48(2):2191–2205
23. Issa M, Elbaset AA, Hassanien AE, Ziedan I (2019) PID controller tuning parameters using meta-heuristics algorithms: comparative analysis. Machine learning paradigms: theory and application, 413–430.
24. Sharma A, Sharma A, Averbukh M, Jately V, Rajput S, Azzopardi B, Lim WH (2023) Performance investigation of state-of-the-art metaheuristic techniques for parameter extraction of solar cells/module. Sci Rep 13(1):11134
25. Lim WH, Sharma A (2023) Overview of swarm intelligence techniques for harvesting solar energy. In: Recent advances in energy harvesting technologies (pp. 161–175). River Publishers
26. Issa M, Samn A (2022) Passive vehicle suspension system optimization using Harris Hawk optimization algorithm. Math Comput Simul 191:328–345
27. Shams-Shemirani S, Tavakkoli-Moghaddam R, Amjadian A, Motamedi-Vafa B (2024) Simulation and process mining in a cross-docking system: a case study. Int J Prod Res 62(13):4902–4925
28. Issa M (2018) Digital image watermarking performance improvement using bio-inspired algorithms. Advances in soft computing and machine learning in image processing, 683–698
29. Ali M, El-Hameed MA, Farahat MA (2017) Effective parameters' identification for polymer electrolyte membrane fuel cell models using grey wolf optimizer. Renew Energy 111:455–462
30. Gupta J, Nijhawan P, Ganguli S (2021) Optimal parameter estimation of PEM fuel cell using slime mould algorithm. Int J Energy Res 45(10):14732–14744
31. Abaza A, El-Sehiemy RA, Mahmoud K, Lehtonen M, Darwish MM (2021) Optimal estimation of proton exchange membrane fuel cells parameter based on coyote optimization algorithm. Appl Sci 11(5):2052
32. Jangir P, Ezugwu AE, Arpita Agrawal SP, Pandya SB, Parmar A, ... Abualigah L (2024) Precision parameter estimation in proton exchange membrane fuel cells using depth information enhanced differential evolution. Sci Rep 14(1):29591
33. Xuebin L, Zhao J, Daiwei Y, Jun Z, Wenjin Z (2024) Parameter estimation of PEM fuel cells using metaheuristic algorithms. Measurement 237:115302
34. Mossa MA, Kamel OM, Sultan HM, Diab AAZ (2021) Parameter estimation of PEMFC model based on Harris Hawks' optimization and atom search optimization algorithms. Neural Comput Appl 33:5555–5570
35. Cao Y, Kou X, Wu Y, Jermsittiparsert K, Yildizbasi A (2020) PEM fuel cells model parameter identification based on a new improved fluid search optimization algorithm. Energy Rep 6:813–823
36. Sharma P, Raju S, Salgotra R (2024) An evolutionary multi-algorithm based framework for the parametric estimation of proton exchange membrane fuel cell. Knowledge-Based Systems 283:111134
37. Fathy A, AbdElaziz M, Alharbi AG (2020) A novel approach based on hybrid vortex search algorithm and differential evolution for identifying the optimal parameters of PEM fuel cell. Renew Energy 146:1833–1845
38. Sharma A, Khan RA, Sharma A, Kashyap D, Rajput S (2021) A novel opposition-based arithmetic optimization algorithm for parameter extraction of PEM fuel cell. Electronics 10(22):2834
39. Salgotra R, Sharma P, Raju S (2024) A multi-hybrid algorithm with shrinking population adaptation for constraint engineering design problems. Comput Methods Appl Mech Eng 421:116781
40. Khajuria R, Bukya M, Lamba R, Kumar R (2024) Optimal parameter extraction of PEM fuel cell using a hybrid weighted mean of vectors and Nelder-Mead simplex method. IEEE Access. https://doi.org/10.1109/ACCESS.2024.3453594
41. Saad B, El-Sehiemy RA, Hasanie HM, El-Dabah MA (2025) Robust parameter estimation of proton exchange membrane fuel cell using Huber loss statistical function. Energy Convers Manage 323:119231
42. Fathy A, Abdel Aleem SH, Rezk H (2021) A novel approach for PEM fuel cell parameter estimation using LSHADE-EpSin optimization algorithm. Int J Energy Res 45(5):6922–6942
43. Hachana O (2022) Accurate PEM fuel cells parameters estimation using hybrid artificial bee colony differential evolution shuffled complex optimizer. Int J Energy Res 46(5):6383–6405
44. Li J, Gao X, Cui Y, Hu J, Xu G, Zhang Z (2020) Accurate, efficient and reliable parameter extraction of PEM fuel cells using shuffled multi-simplexes search algorithm. Energy Convers Manage 206:112501
45. Zheng J, Xie Y, Huang X, Wei Z, Taheri B (2021) Balanced version of slime mold algorithm: a study on PEM fuel cell system parameters identification. Energy Rep 7:3199–3209
46. Abdel-Basset M, Mohamed R, Elhoseny M, Chakrabortty RK, Ryan MJ (2021) An efficient heap-based optimization algorithm for parameters identification of proton exchange membrane fuel cells model: analysis and case studies. Int J Hydrogen Energy 46(21):11908–11925
47. Yang Z, Liu Q, Zhang L, Dai J, Razmjooy N (2020) Model parameter estimation of the PEMFCs using improved barnacles mating optimization algorithm. Energy 212:118738
48. Houssein EH, Helmy BED, Rezk H, Nassef AM (2021) An enhanced Archimedes optimization algorithm based on local escaping operator and orthogonal learning for PEM fuel cell parameter identification. Eng Appl Artif Intell 103:104309
49. Rezk H, Ferahtia S, Djeroui A, Chouder A, Houari A, Machmoum M, Abdelkareem MA (2022) Optimal parameter estimation strategy of PEM fuel cell using gradient-based optimizer. Energy 239:122096
50. Riad AJ, Hasanien HM, Turky RA, Yakout AH (2023) Identifying the PEM fuel cell parameters using artificial rabbits optimization algorithm. Sustainability 15(5):4625
51. Messaoud RB, Midouni A, Hajji S (2021) PEM fuel cell model parameters extraction based on moth-flame optimization. Chem Eng Sci 229:116100
52. Mujeer SA, Chandrasekhar Y, Kumari MS, Salkuti SR (2024) An accurate method for parameter estimation of proton exchange membrane fuel cell using dandelion optimizer. Int J Emerg Electr Power Syst 25(3):333–344
53. Gouda EA, Kotb MF, El-Fergany AA (2021) Jellyfish search algorithm for extracting unknown parameters of PEM fuel cell models: steady-state performance and analysis. Energy 221:119836
54. Han W, Li D, Yu D, Ebrahimian H (2023) Optimal parameters of PEM fuel cells using chaotic binary shark smell optimizer. Energy Sources Part A Recov Util Environ Eff 45(3):7770–7784
55. Shaheen A, El-Sehiemy R, El-Fergany A, Ginidi A (2023) Fuel-cell parameter estimation based on improved gorilla troops technique. Sci Rep 13(1):8685
56. BaradaranRezaei H, Amjadian A, Sebt MV, Askari R, Gharaei A (2023) An ensemble method of the machine learning to prognosticate the gastric cancer. Ann Oper Res 328(1):151–192
57. Ragab M, Alshammari SM, Al-Ghamdi AS (2023) Modified metaheuristics with weighted majority voting ensemble deep learning model for intrusion detection system. Computer Syst Sci Eng 47(2)
58. Fonseca GB, Nogueira TH, Ravetti MG (2019) A hybrid Lagrangian metaheuristic for the cross-docking flow shop scheduling problem. Eur J Oper Res 275(1):139–154
59. Gharaei A, Amjadian A, Shavandi A, Amjadian A (2023) An augmented Lagrangian approach with general constraints to solve nonlinear models of the large-scale reliable inventory systems. J Comb Optim 45(2):78

60. Mishra NS, Dhabal S (2024) An improved hybrid fusion of noisy medical images using differential evolution-based artificial rabbits optimization algorithm. Multidimens Syst Signal Process 35(2):83–137
61. Sultan HM, Menesy AS, Hassan MS, Jurado F, Kamel S (2023) Standard and quasi oppositional bonobo optimizers for parameter extraction of PEM fuel cell stacks. Fuel 340:127586
62. Menesy AS, Sultan HM, Selim A, Ashmawy MG, Kamel S (2019) Developing and applying chaotic Harris hawks optimization technique for extracting parameters of several proton exchange membrane fuel cell stacks. IEEE Access 8:1146–1159
63. Chen Y, Zhang G (2022) New parameters identification of proton exchange membrane fuel cell stacks based on an improved version of African vulture optimization algorithm. Energy Rep 8:3030–3040
64. Hasanien HM, Shaheen MA, Turky RA, Qais MH, Alghuwainem S, Kamel S, Jurado F (2022) Precise modeling of PEM fuel cell using a novel enhanced transient search optimization algorithm. Energy 247:123530
65. Ahmadianfar I, Heidari AA, Gandomi AH, Chu X, Chen H (2021) Run beyond the metaphor: an efficient optimization algorithm based on Runge Kutta method. Expert Syst Appl 181:115079
66. Heidari AA, Mirjalili S, Faris H, Aljarah I, Mafarja M, Chen H (2019) Harris hawks optimization: algorithm and applications. Futur Gener Comput Syst 97:849–872
67. Su H, Zhao D, Heidari AA, Liu L, Zhang X, Mafarja M, Chen H (2023) RIME: a physics-based optimization. Neurocomputing 532:183–214
68. Zitar RA, Al-Betar MA, Awadallah MA, Doush IA, Assaleh K (2022) An intensive and comprehensive overview of JAYA algorithm, its versions and applications. Arch Comput Methods Eng 29(2):763–792
69. Shan R, Rezaei T (2021) Lung cancer diagnosis based on an ANN optimized by improved TEO algorithm. Comput Intell Neurosci 2021(1):6078524
70. Ahmadianfar I, Heidari AA, Noshadian S, Chen H, Gandomi AH (2022) Info: an efficient optimization algorithm based on weighted mean of vectors. Expert Syst Appl 195:116516
71. Shehab M, Abualigah L, Al Hamad H, Alabool H, Alshinwan M, Khasawneh AM (2020) Moth–flame optimization algorithm: variants and applications. Neural Comput Appl 32(14):9859–9884
72. Abualigah L, Yousri D, AbdElaziz M, Ewees AA, Al-Qaness MA, Gandomi AH (2021) Aquila optimizer: a novel meta-heuristic optimization algorithm. Comput Ind Eng 157:107250
73. Wang D, Tan D, Liu L (2018) Particle swarm optimization algorithm: an overview. Soft Comput 22(2):387–408
74. Rowe A, Li X (2001) Mathematical modeling of proton exchange membrane fuel cells. J Power Sources 102(1–2):82–96
75. Corrêa JM, Farret FA, Canha LN, Simoes MG (2004) An electrochemical-based fuel-cell model suitable for electrical engineering automation approach. IEEE Trans Ind Electron 51(5):1103–1112
76. Aouali FZ, Becherif M, Ramadan HS, Emziane M, Khellaf A, Mohammedi K (2017) Analytical modelling and experimental validation of proton exchange membrane electrolyser for hydrogen production. Int J Hydrogen Energy 42(2):1366–1374
77. Amphlett JC, Baumert RM, Mann RF, Peppley BA, Roberge PR, Harris TJ (1995) Performance modeling of the Ballard Mark IV solid polymer electrolyte fuel cell: I. mechanistic model development. J Electrochem Soc 142(1):1
78. Amphlett JC, Baumert RM, Mann RF, Peppley BA, Roberge PR, Harris TJ (1995) Performance modeling of the Ballard Mark IV solid polymer electrolyte fuel cell: II. Empirical model development. J Electrochem Soc 142(1):9
79. Mo ZJ, Zhu XJ, Wei LY, Cao GY (2006) Parameter optimization for a PEMFC model with a hybrid genetic algorithm. Int J Energy Res 30(8):585–597
80. Alatas B (2010) Chaotic harmony search algorithms. Appl Math Comput 216(9):2687–2699
81. Nguyen TV, White RE (1993) A water and heat management model for proton-exchange-membrane fuel cells. J Electrochem Soc 140(8):2178
82. El-Fergany AA (2018) Electrical characterisation of proton exchange membrane fuel cells stack using grasshopper optimiser. IET Renew Power Gener 12(1):9–17
83. Das S, Suganthan PN (2010) Differential evolution: a survey of the state-of-the-art. IEEE Trans Evol Comput 15(1):4–31
84. Das S, Mullick SS, Suganthan PN (2016) Recent advances in differential evolution–an updated survey. Swarm Evol Comput 27:1–30
85. Wang L, Cao Q, Zhang Z, Mirjalili S, Zhao W (2022) Artificial rabbits optimization: a new bio-inspired meta-heuristic algorithm for solving engineering optimization problems. Eng Appl Artif Intell 114:105082
86. Ahmad MF, Isa NAM, Lim WH, Ang KM (2022) Differential evolution: a recent review based on state-of-the-art works. Alex Eng J 61(5):3831–3872
87. Zhang Y, Huang C, Huang H, Wu J (2023) Multiple learning neural network algorithm for parameter estimation of proton exchange membrane fuel cell models. Green Energy and Intelligent Transportation 2(1):100040
88. Waseem M, Amir M, Lakshmi GS, Harivardhagini S, Ahmad M (2023) Fuel cell-based hybrid electric vehicles: an integrated review of current status, key challenges, recommended policies, and future prospects. Green Energy and Intelligent Transportation 2(6):100121
89. Qiu Y, Zeng T, Zhang C, Wang G, Wang Y, Hu Z, ... Wei Z (2023) Progress and challenges in multi-stack fuel cell system for high power applications: architecture and energy management. Green Energy Intell Transp 2(2):100068
90. Liu C, Chen Y, Xu R, Ruan H, Wang C, Li X (2024) Co-optimization of energy management and eco-driving considering fuel cell degradation via improved hierarchical model predictive control. Green Energy and Intelligent Transportation 3(6):100176

Authors and Affiliations

Manish Kumar Singla[1,2] · Mohammad Aljaidi[3] · Pradeep Jangir[4,5] · Arpita[1] · Ramesh Kumar[6] · Reena Jangid[7,8]

✉ Manish Kumar Singla
msingla0509@gmail.com

Mohammad Aljaidi
mjaidi@zu.edu.jo

Pradeep Jangir
pkjmtech@gmail.com

Arpita
apyjangid@gmail.com

Ramesh Kumar
rameshkumarmeena@gmail.com

Reena Jangid
reenajangidiitm@gmail.com

[1] Department of Biosciences, Saveetha School of Engineering, Saveetha Institute of Medical and Technical Sciences, Chennai 602 105, India

[2] Applied Science Research Centre, Applied Science Private University, Amman 11937, Jordan

[3] Department of Computer Science, Faculty of Information Technology, Zarqa University, Zarqa 13110, Jordan

[4] Research and Innovation Cell, Rayat Bahra University, Mohali 140301, Punjab, India

[5] Jadara University Research Center, Jadara University, Irbid 21110, Jordan

[6] Department of Interdisciplinary Courses in Engineering, Chitkara University Institute of Engineering & Technology, Chitkara University, Punjab 140401, India

[7] Department of CSE, Graphic Era Hill University, Dehradun 248002, Uttarakhand, India

[8] Department of CSE, Graphic Era Deemed To Be University, Dehradun 248002, Uttarakhand, India